**Department of the Environment,
Transport and the Regions
Commissioned research for Radioactive Substances Division**

Experimental Measurements and Computer Simulation of Fission Product Gamma-ray Spectra.

Report No: DETR/RAS/97.002

Contract Title: Characterisation of the response of airborne systems to short-lived fission products.

DETR Reference: RW 8/6/72 **Sector:** C, D

Authors:
D.C.W. Sanderson, A.J. Cresswell, J.D. Allyson, P. McConville
Scottish Universities Research and Reactor Centre, East Kilbride, G75 0QF

Date approved by DETR: September 1997

Abstract:
Airborne gamma ray spectrometry using high volume scintillation detectors, optionally in conjunction with Ge detectors, has potential for making rapid environmental measurements in response to nuclear accidents. An experimental investigation and computer simulation have been used to characterise the response of such detectors to short lived fission products. Small samples of ^{235}U were irradiated in a research reactor for short periods, to generate fission product sources. Gamma ray spectra were recorded over a period of one year using both high volume scintillation detectors and semiconductor detectors. The main gamma emitting nuclides have been identified, and their associated signals in each detector defined. Simulation work has been used to calculate the corresponding spectra which would have been observed at airborne survey heights, or from fission product sources irradiated for a prolonged period. While Ge detectors can record a fuller range of isotopes, of interest in characterising release terms, the NaI spectra also have potential for providing data on a range of radiologically important isotopes at all stages.

SUMMARY

Airborne Gamma Spectrometry (AGS) has developed considerably in recent years, and is recognised as having an important contribution to make to nuclear emergency response. The abilities to survey large areas rapidly with high sampling densities, and to produce radiometric maps on emergency timescales have already been demonstrated. However the ability of AGS systems to resolve complex gamma spectra in the early phases of a reactor accident is less well defined. An earlier report (Sanderson et. al. 1997) reviewed experience from past nuclear accidents, together with source terms and AGS spectra recorded. This report presents results of an experimental and computational investigation of the response of AGS systems to short lived fission products.

An experiment was conducted in which small, sealed samples of ^{235}U were irradiated in the UTR-300 research reactor in East Kilbride, producing unseparated fission product sources. Gamma ray spectra were recorded, under laboratory conditions from these sources over a one year period using a high volume (16l) sodium iodide (NaI) spectrometer and two types of Germanium (Ge) detectors. The Ge spectra, together with a numerical simulation of the fission process, were used to identify the main gamma emitting isotopes present at each stage, and their contributions to the NaI spectra recorded. Some 42 isotopes were identified in the initial Ge spectra, but this reduced to 20 after one week, and 7 after six months.

The spectra recorded using the NaI detectors contain several composite peaks, which although unable to resolve the full set of nuclides, could provide information on radiologically important isotopes at all stages. The extent of interferences in the NaI spectra, and the need for spectral stripping were examined. Under accident conditions, where volatile and non-volatile species are expected to be separated from each other to a greater extent than revealed in this experiment, the extent of spectral interferences would be reduced. From the data it has been noted that NaI spectra could provide information on the following groups of isotopes. Sr isotopes might be inferred over the first day following accident using ^{91}Sr and ^{92}Sr, providing the release and AGS mobilisation take place rapidly after irradiation. Iodine nuclides would be measurable over the first few weeks, initially using ^{134}I (first day only), ^{133}I and ^{135}I (first 2 days); thereafter $^{132}I/^{132}Te$ (first week or so), and ^{131}I (first 2-3 weeks). The extent to which Cs isotopes can be quantified during the early stages depends on the fuel age of the reactor, and on the extent of separation of volatile and non-volatile products during the release phase. Finally non-volatile products such as $^{95}Zr/^{95}Nb$, ^{99}Mo, ^{140}La, would be detectable for significant periods following release, again their relative contributions depending on the accident scenario.

A computer model was developed to simulate the fission product inventories and resulting NaI spectra for these experiments, in both close-coupled and airborne observational geometries. The agreement between simulation and experiment was good. These models were also used to investigate the influence of prolonged irradiation on gamma spectra. As expected this modified the predicted results. These models could be used to simulate the response of AGS systems to past accidents and reference accidents for current reactors.

The experiment has confirmed that AGS systems could provide useful information under accident conditions, given a suitable combination of detectors, and appropriate spectral analysis.

ACKNOWLEDGEMENTS

The work described here is part of a project supported by the Department of the Environment, Transport and the Regions (project DOE RW 8/6/72) and the Ministry of Agriculture, Fisheries and Food (project MAFF RP0237).

The samples of ^{235}U used in the experiment were supplied by AEA Technology (ref. no. AE 7159).

CONTENTS

1. INTRODUCTION

1.1 Aims

This report sets out the findings of an experimental and computational investigation into the response of airborne gamma-ray spectrometry (AGS) systems to the accidental release of fission products, with particular reference to shorter lived radioisotopes. A review of past nuclear accidents has been reported (Sanderson et. al. 1997), detailing source terms for those accidents with major off-site releases and summarising general features of γ-ray spectra observed after these accidents. The influences of the timing of the release, relative to reactor operation, and of segregation of volatile and non-volatile radionuclides during and after release, in determining the isotopic composition of deposited radioactivity were noted. Delays in employing AGS surveys and the types of systems used have limited the extent to which the practical experience gained in response to past accidents reflects the full range of potential behaviour. The experimental and computational simulations reported here aim to complement existing experience and to provide a systematic basis for evaluating the contribution AGS can make to emergency response.

The experimental investigation used small ^{235}U sources irradiated and measured under laboratory conditions, sealed within a silica ampoule to retain the full suite of fission products, and representing close coupled source to detector geometries. This has provided a set of γ-ray spectra recorded using AGS detector systems, including both high volume scintillation and high resolution semi-conductor detectors, from fission product sources over a one year period.

Computational models, consisting of source term simulations coupled to Monte Carlo calculations for detector response, have been developed to simulate the experimental results. Comparison between the experimental and simulated spectra has been used to verify the code, and assist in the identification of features in the experimental spectra. The simulation has then been applied to investigate the relationship between measured laboratory spectra and full scale airborne geometry, and the effect of prolonged irradiation on γ-ray spectra.

The combination of spectra measured following past nuclear accidents, the experimental and simulated data sets, has been used to assess the extent to which high volume sodium iodide (NaI) detectors can deal with complex fission product spectra. These data sources are also useful for the development of strategies for data analysis appropriate to use in the early stages of emergency response, and for evaluating features which should be taken into account in the design of new AGS systems (eg: the need for Ge detectors).

1.2 Fission product gamma-rays

Nuclear fission results in the production of several hundred nuclides, most of which are unstable to beta-decay and result in isobaric decay chains. Typically, fission directly populates the more neutron rich end of each decay chain, with the population of the more stable isotopes in the chain resulting from β-decay. The cumulative fission yield (the sum of the independent yields as a result of direct fission population and the decay of parents) is greater than 0.1% for 125 isotopes with half lives longer than one hour, 45 of which are stable. The higher yield isotopes will be more abundant in an undifferentiated nuclear fission source.

The isotopes expected to contribute to γ-ray spectra of fission sources can be predicted from nuclear data. Only fairly long lived nuclides would be expected to contribute to the source, except for periods very shortly after fission. So only isotopes with half lives in excess of one hour are considered here, with a few exceptions where the isotope is a decay product of a longer lived parent.

The activity, *A*, in units of Bq per fission, due to a particular isotope is given by

$$A = \lambda Y_f \tag{1.1}$$

where Y_f is the cumulative fission yield and $\lambda = ln2/t_{½}$ is the decay constant, where $t_{½}$ is the half life in seconds. For daughter isotopes with half-lives less than their parents the half-life of the parent isotope was used. This represents the activity at time zero (ie: immediately following fission) and assumes all the parent nuclei decay instantaneously. It also assumes that none of the isotopes have had a chance to reach equilibrium. As such, this approximates to the activities for real fission sources such as irradiated nuclear fuel.

The number of γ-rays per second per fission, A_γ is given by

$$A_\gamma = A I_\gamma \tag{1.2}$$

where I_γ is the γ-ray yield. The γ-activity will decrease with time following the radioactive decay law, with only the most intense γ-rays at any time contributing significantly to the γ-spectrum. Table 1.1 lists the most intense γ-emitting fission products sorted in half-life order with their principal γ-rays. It would be expected that these nuclei will be observed in fission product γ-ray spectra measured over various times since fission, with the more intense short-lived products decaying out of the source to allow the less intense longer-lived products to dominate at later stages. In generating this table a minimum threshold for the activity A_γ was used to eliminate low intensity nuclei, this threshold was set at 10^{-7} for isotopes with half-lives of the order of a few hours, and decreased with increasing half-life to 10^{-10} for isotopes with half-lives in excess of a year.

In addition to these γ-emitting isotopes, which under favourable circumstances may be detectable by AGS or other γ-ray spectrometry methods, there are also a number of fission products which either do not emit γ-rays or only emit very weak or low energy γ-rays. Most of these are β-emitters, although a few higher mass isotopes decay by α-emission. Table 1.2 lists some of the longer lived high yield nuclides with their half lives, cumulative fission yields, activities and β-decay Q-values (the maximum energy available to the β-particle). These isotopes are likely to persist in the environment and contribute significantly to radiation dose, some (particularly the Sr isotopes) are of particular concern because of their potential biological importance.

Nuclide	Half life	Cumulative yield (%)	Activity, A (10^{-6} Bq/fission)	Principal gamma-rays		Comments
				Energy (keV)	A_γ (10^{-6} γ/fission/s)	
^{87}Kr	1.27h	2.5	3.8	402.58	1.9	
^{139}Ba	1.38h	6.5	9.1	165.86	2.2	
^{142}La	1.52h	5.8	7.3	641.29 2397.8 2542.7	3.5 0.98 0.73	
^{149}Nd	1.73h	1.0	1.1	114.31 211.31 270.17	0.21 0.29 0.12	
^{92}Sr	2.71h	6.0	4.3	1383.9	3.8	
^{88}Kr	2.84h	3.5	2.4	196.32 834.83 1529.77 2195.84 2392.11	0.62 0.31 0.26 0.31 0.82	
^{88}Rb	17.8m	3.5	2.4	898.0 1836	0.34 0.51	^{88}Kr daughter
^{92}Y	3.54h	6.0	3.3	934.5	0.45	
^{141}La	3.93h	5.9	2.9	1354.52	0.075	
^{129}Sb	4.40h	0.72	0.39	544.7 812.8 914.6 1030.1	0.070 0.17 0.078 0.049	
^{105}Ru	4.44h	0.96	0.42	316.44 469.37 676.36 724.3	0.046 0.073 0.065 0.20	
^{85m}Kr	4.48h	1.3	0.56	151.18 304.87	0.42 0.078	
^{135}I	6.61h	6.3	1.8	1131.5 1260.4	0.42 0.53	
^{135}Xe	9.09h	6.6	1.4	249.79	1.3	
^{91}Sr	9.52h	5.9	1.2	749.8 1024.3	0.28 0.40	
^{91m}Y	49.71m	2.9	0.59	555.6	0.57	^{91}Sr daughter
^{93}Y	10.10h	6.3	1.2	266.87	0.082	
^{97}Zr	16.90h	6.0	0.68	507.66 1147.99	0.036 0.018	
^{97}Nb	1.20h	6.0	0.68	657.92	0.67	^{97}Zr daughter

^{97m}Nb	1.00m	5.7	0.65	743.36	0.64	^{97}Zr daughter
^{133}I	20.80h	6.6	0.61	529.87	0.53	
^{151}Pm	1.18d	0.42	0.029	340.1	0.0065	
^{143}Ce	1.38d	5.9	0.34	57.37 293.26	0.040 0.14	
^{105}Rh	1.47d	0.96	0.052	318.9	0.010	
^{99}Mo	2.75d	6.2	0.18	739.5	0.022	
^{99m}Tc	6.02h	5.4	0.16	140.47	0.14	^{99}Mo daughter
^{132}Te	3.26d	4.2	0.10	228.16	0.091	
^{132}I	2.30h	4.3	0.11	522.65 630.22 667.67 772.6 954.55	0.017 0.014 0.10 0.081 0.019	^{132}Te daughter
^{133}Xe	5.25d	6.6	0.10	81	0.037	
^{131}I	8.04d	2.9	0.029	364.48	0.023	
^{147}Nd	10.98d	2.3	0.017	91.11 531.02	0.0047 0.0022	
^{140}Ba	12.74d	6.3	0.040	537.27	0.0097	
^{140}La	1.68d	6.3	0.040	328.77 487.03 815.78 1596.17	0.0082 0.018 0.0094 0.038	^{140}Ba daughter
^{141}Ce	32.50d	5.9	0.015	145.44	0.0070	
^{103}Ru	39.35d	3.0	0.0061	497.08	0.0054	
^{95}Zr	63.98d	6.6	0.0083	724.23 756.74	0.0037 0.0045	
^{95}Nb	35.15d	6.6	0.0083	765.83	0.0083	^{95}Zr daughter
^{144}Ce	184.90d	5.5	0.0024	133.52	0.00026	
^{106}Ru	1.007y	4.1	0.00089			
^{106}Rh	29.8s	4.1	0.00089	511.86	0.00019	^{106}Ru daughter
^{137}Cs	30.00y	6.2	0.000045	661.65	0.000039	^{137m}Ba γ-ray

Table 1.1: The cumulative yields, activities and principal γ-rays for the most γ-intense fission products, sorted in half-life order. It would be expected that these isotopes would be detectable by AGS or other γ-ray spectrometry methods in a nuclear fission source.

Nuclide	Half life	Cumulative yield (%)	A (10^{-6} Bq/fission)	β Q-value (MeV)	Comments
^{89}Sr	50.5d	4.8	0.0076	1.492	no γ
^{90}Sr	29.12y	5.8	0.000044	0.546	no γ
^{90}Y	2.67d	5.8	0.000044	2.284	very weak γ
^{91}Y	58.51d	5.9	0.0081	1.543	very weak γ
^{143}Pr	13.58d	5.9	0.035	0.935	very weak γ
^{145}Pr	5.98h	3.9	1.3	1.805	very weak γ
^{147}Pm	2.62y	2.2	0.00018	0.225	very weak γ
^{149}Pm	2.21d	1.0	0.036	1.072	very weak γ

Table 1.2: The half-life, cumulative yield, activity and β-decay Q-value for some high yield, longer lived fission products not detectable by γ-ray spectrometry.

2. EXPERIMENTAL MEASUREMENTS

2.1 Overview

The experiment consisted of a fission product source and three γ-ray detectors; the 16 litre NaI detector from the AGS system, a 50% efficiency Ge detector (GMX) and a thin crystal Ge (LoAx) detector. These detectors recorded spectra using two different spectrometry systems. The spectra recorded by the GMX and NaI detectors were recorded using the AGS rack. The GMX spectra were also recorded using an Ortec 919 buffer along with the LoAx spectra.

The source consisted of one or more samples of ^{235}U that had been irradiated in the SURRC UTR 300 research reactor. Five samples were prepared, each of which was irradiated for different periods. The source was placed on a plinth, with the sample(s) and source-detector distance selected so as maximize counting statistics without producing excessive dead time in the NaI detector system.

Spectra were recorded at various times over a one year period after the sources were irradiated. In excess of 20 000 spectra were recorded using the three detector systems. Peaks in representative Ge spectra were identified from their energies using γ-ray energy and intensity information from the JEF 2.2 database (OECD 1994), the compositions of peaks in the corresponding NaI spectra were then determined using these identifications. These assignments were confirmed by measuring the decay of these peaks through the entire NaI data set. From this information the major contributions to the NaI γ-ray spectra at various stages during the decay were determined.

2.2 Source Preparation

A solution of 5.06±0.03 cm^3 of ^{235}U tracer in 6.66±0.03 g of 8M HNO_3 was obtained from AEA Technology (Reference No. AE 7159, type 92/235/88). The U concentration in this solution was specified as 317.3±1.6 µg U per gram of solution, with the measured isotopic composition being 0.836±0.008% ^{234}U, 92.49±0.02% ^{235}U, 0.334±0.003% ^{236}U, and 6.338±0.006% ^{238}U. Therefore, the concentration of ^{235}U in the solution was 293.5±1.6 µg/g.

Five portions of this solution were dispensed into 8mm external diameter silica tubes with a target volume of 0.77569 cm^3, equivalent to 1.022g of solution or 300 µg of ^{235}U. The contents of the tubes were evaporated to dryness and then the tubes flame sealed. During the process some loss of nitric acid solution may have occurred, and therefore the 300 µg ^{235}U content of each sample is an upper limit. At the same time, four empty tubes were prepared and sealed, one of which was subjected to prolonged heating to verify it's containment integrity.

The samples were irradiated on 11th September 1995 in the SURRC UTR 300 research reactor, at a nominal neutron flux of 2.3×10^{12} n s^{-1}. For 300 µg of ^{235}U this would result in an estimated 1.0×10^9 fissions per second. Along with the samples, each irradiation also contained a blank sample, to enable activation products from the tubes to be discounted from the measured spectra, and two gold foil flux monitors held in small eppendorf capsules placed over each end of the tube. The samples and flux monitors were double contained in zipseal polythene bags. Table 2.1 gives

Source	Mass before drying (g)	Time in reactor (s)
A	1.052	40
B	1.032	400
C	1.072	5620
D	1.076	5620
E	1.021	5620

Table 2.1: The mass (before drying) and irradiation time for each of the five samples.

the mass of solution prior to drying and the irradiation time for each of the five samples.

The fission sources thus produced are not entirely representative of nuclear accident source terms. The sources produced experimentally were sealed, and so there is no physical or chemical separation of the isotopes present. In particular they contain inert gases, which although released in an accident are not deposited, and relatively large amounts of refractory elements which would be less preferentially released in an accident situation. They also contain no activation products from fuel cladding and reactor components. In addition, the sources were irradiated for relatively short times compared to the irradiation times for most accident scenarios. Thus the shorter lived isotopes will have had less time to reach equilibrium, and so be relatively abundant compared with the longer lived isotopes, and the production of higher actinides, which have slightly different fission product yields, would have been small.

2.3 Experimental Arrangement

The 16 litre NaI detector was placed on top of a bench 92cm above the floor, with the crystal ends approximately 17cm laterally displaced from the source which was placed 67cm down the laboratory floor pit (a source-NaI distance of 164cm). The GMX detector was placed on the floor, with its centre line approximately 80cm below the NaI detector, overhanging the pit. For the first set of measurements only these two detectors were used, with spectra being logged by the AGS computer rack.

For the rest of the experiment, spectra were also recorded from the LoAx and GMX detectors through an Ortec 919 buffer. These two detectors were placed on the floor, and the NaI detector was moved so that the centre of the detector was directly above the source. For most of the remaining measurements the source was placed on a polystyrene plinth either 60 or 68cm below the NaI detector, with the lateral displacement of the Ge detectors from the vertical axis of the source being 20cm for the LoAx detector and 30cm for the GMX. This arrangement is shown schematically in figure 2.1. As the sources decayed combinations of sources were used to increase counting statistics. For a few sets of measurements, the source was again placed in the floor pit, and the Ge detectors moved to overhang it.

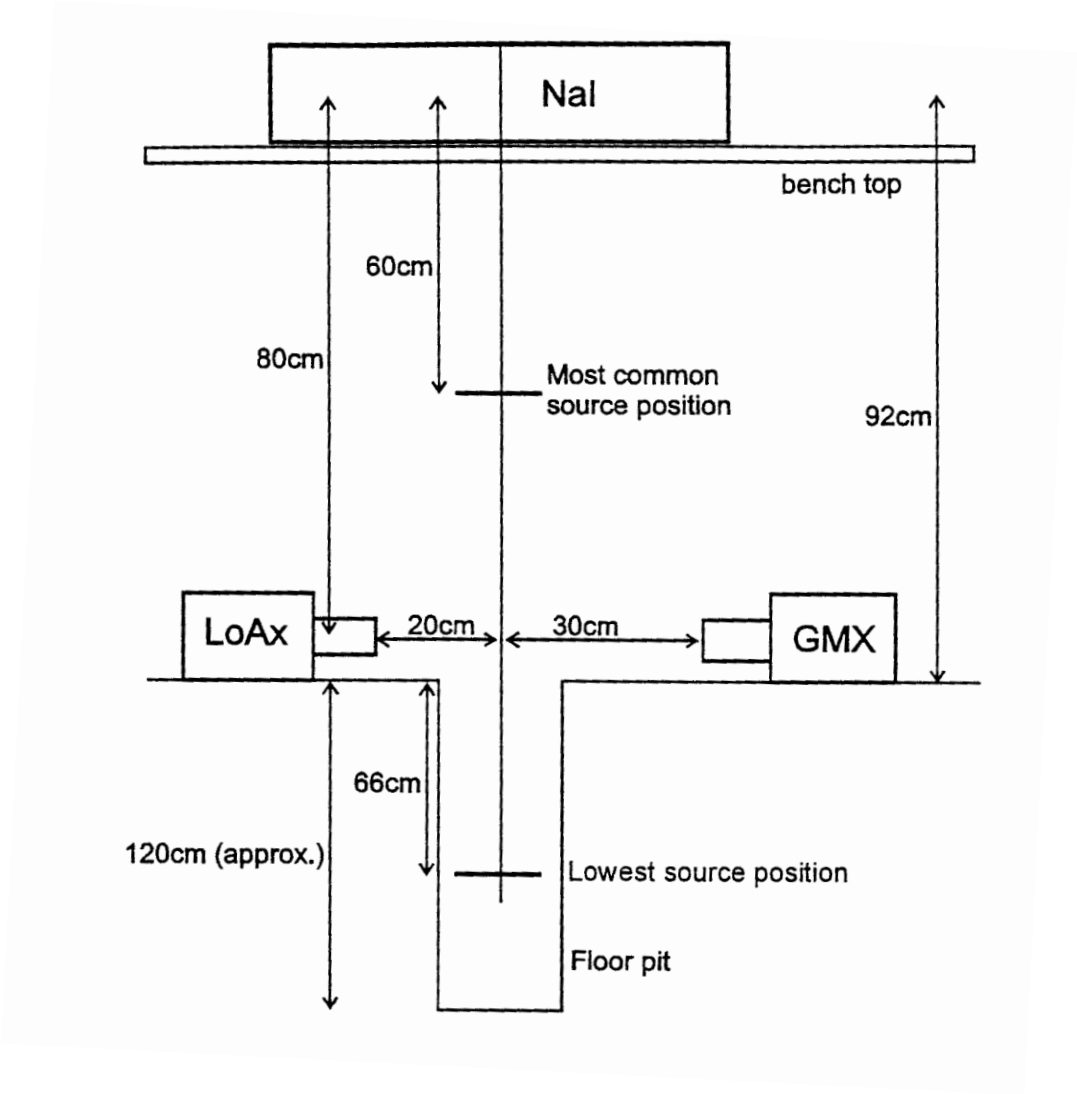

Figure 2.1: Schematic of the detector arrangement (not to scale) with the most used source position and the lowest source position marked. With the source placed in the floor pit the Ge detectors were positioned overhanging the pit. For the initial run, the LoAx detector was not used and the NaI detector was offset with the ends of the crystals 17cm from the vertical axis of the source.

Spectra from the NaI and GMX detectors were logged using the AGS computer rack. This consists of instrumentation power supply, EHT power supply for the detectors, spectroscopic amplifiers and a pulse height analyser connected to a PC running data acquisition software developed for the collection and integration, using pre-defined spectral windows, of γ-ray spectra using the NaI detector, with the option of using additional Ge detectors. This software stores the NaI spectra in 512 channels at approximately 6 keV per channel and the Ge spectra in 2048 channels at approximately 1.5 keV per channel. Lower thresholds were set to limit dead-time in the spectrometers due to x-rays and lower energy scattered photons. For most of the measurements both detectors recorded γ-rays in the range of ≈20-3000 keV, although for some of the later measurements the NaI detector threshold was set higher.

The spectra from the LoAx and GMX detectors were logged from an Ortec 919 "Spectrum Master" using the Ortec Maestro software. The signals from the detector pre-amplifiers were

processed by spectroscopic amplifiers before being fed into the 919 buffer. They were logged as 8k spectra at approximately 0.4 keV per channel for the GMX and as 2k spectra at approximately 0.5 keV per channel for the LoAx detector. The LoAx spectra were recorded in the range ≈15-1000 keV, and the GMX spectra in the range ≈30-3000 keV.

2.4 Measurements Taken

Over the course of a year spectra were recorded from the sources using these detectors. Details of each of these sets of measurements are given in Appendix A. In total the AGS system recorded 7350 GMX and 14700 NaI spectra, of which approximately 80% were recorded with a fission source in place, the remainder being background or calibration spectra. The Ortec 919 buffer recorded 750 GMX and LoAx spectra.

2.5. Spectral Analysis

The high resolution spectra recorded using the LoAx and GMX detectors were studied first. It was possible to determine the energies of the peaks in these spectra to high accuracy, and from comparisons with nuclear data tables of γ-ray energies assign most of them to particular radioisotopes. The peaks in the Ge spectra were then used to identify the components of peaks in the NaI spectra. The composition of these peaks was then confirmed by studying the decay of these peaks over time, and hence determining half-lives of the contributing components.

For both sets of data some pre-processing was required to account for gain shift, and to subtract the laboratory background. This has resulted in the development of several simple data processing routines for use with spectra recorded with the AGS system.

It was noted that the gain of the NaI detector drifted considerably during the various sets of measurements, following diurnal and weekly cycles with gain maxima at night and over weekends. A gain correction routine, based on the DRIFT routine of Paatero 1964, was used to shift and stretch the spectra to 6 keV per channel using the ^{40}K (1460.8 keV) and ^{208}Tl (2614.53 keV) peaks as references. Details of this are given in Appendix B.

Background spectra, either of the laboratory background alone or of the blank silica tubes, were recorded at stages throughout the year measurements were taken. The spectra recorded with the blank tubes were compared to those of the laboratory background alone. There was no discernable difference between the two background data sets, ie: the contribution of any activation products in the tubes to the γ-ray spectra was insignificant.

The background spectra recorded over the year were studied to check detector characteristics and any variation in the laboratory background. The resolution of the detectors logged by the AGS rack and the LoAx detector was fairly constant over the duration of the experiment, however the resolution of the GMX detector logged by the 919 buffer was more variable. For the LoAx detector the FWHM of the ^{214}Pb (351.9 keV) peak was typically 0.9 keV. For the NaI and GMX detectors logged through the AGS rack the FWHMs of the ^{40}K (1460.8 keV) peak were typically 100 keV and 3.3 keV respectively. The FWHM of the ^{40}K peak for the GMX detector logged through the 919 buffer varied between 2.5 keV and 9.3 keV.

The variability of the laboratory background was also studied using the GMX spectra recorded through the 919 buffer. It was found that the count rates due to the U-series, the Th-series and ^{40}K were constant during the course of the experiment. However, the count rate due to ^{137}Cs was variable, usually at about 0.4 cps, but sometimes falling to 0.1 cps and on one occasion rising to 0.9 cps. This was probably due to the use of sources in an adjacent laboratory, or other activities in the laboratory. Study of spectra recorded before, during and after the worst affected spectra indicated that this variability had little effect on the measured fission product spectra.

Any possible variation in the background due to changes in radon concentration was also checked, by taking the ratios of count rates for peaks from isotopes above and below radon in the decay chains. These ratios were constant, indicating that the radon concentration did not vary sufficiently to affect the laboratory background.

The laboratory background recorded closest in time to the fission spectra was subtracted from the measured spectra, to leave residual spectra due solely to fission products. Several of these residual spectra were combined to improve statistics.

2.6 Fission Product Spectra

Fission product spectra for representative times after irradiation were prepared as described above. The energies of the peaks in the Ge spectra were determined, and the γ-rays contributing to the spectra identified by comparison with nuclear data (OECD 1994). The radioisotopes contributing to the NaI peaks were determined by comparison with the concurrently recorded Ge spectra.

Spectra recorded 3 hours after irradiation

The spectra recorded with the GMX and NaI detectors are shown in figure 2.1, the LoAx detector was not used at this time. Gamma-rays from 40 different isotopes were identified in these spectra, with 9 major peaks in the NaI spectrum. Of these, the most prominent is the 864keV peak, composed predominantly of ^{134}I γ-rays. Other NaI peaks of interest include the 1380keV peak which is largely ^{92}Sr and the 1494keV which is almost totally due to ^{135}I and ^{88}Kr. Table 2.1 lists the principal γ-rays observed with the GMX detector, and table 2.2 lists the major peaks in the NaI spectrum with the approximate contributions of different radionuclides.

Spectra recorded 1 day after irradiation

The spectra recorded with the three detector systems are shown in figure 2.2. Gamma-rays from 28 different isotopes were identified in these spectra, with 9 major peaks in the NaI spectrum. Of these, the most prominent is the 516keV peak, which is composed mostly of ^{133}I γ-rays with a significant contribution from ^{91m}Y. Other NaI peaks of interest include the 222keV peak which is composed mostly of ^{135}Xe γ-rays, the 1266keV and 1446keV peaks which are composed mostly of iodine γ-rays and the 1014keV peak which is composed mostly of ^{91}Sr γ-rays. The 342keV peak is due largely to ^{131}I, however it is a fairly small peak that is not fully resolved at this time. Table 2.3 lists the principal γ-rays observed with the Ge detectors, and table 2.4 lists the major peaks in the NaI spectrum with the approximate contributions of different radionuclides.

Spectra recorded 2 days after irradiation

The spectra recorded with the three detector systems are shown in figure 2.3. Gamma-rays from 26 different isotopes were identified in these spectra, with 8 major peaks in the NaI spectrum. Peaks of interest in the NaI spectrum include the 210keV peak composed mostly of ^{132}Te and ^{135}Xe γ-rays, the 510keV peak composed largely of ^{133}I γ-rays and the 1590keV peak which is predominantly due to ^{140}La γ-rays. Table 2.5 lists the principal γ-rays observed with the Ge detectors, and table 2.6 lists the major peaks in the NaI spectrum with the approximate contributions of different radionuclides.

Spectra recorded 1 week after irradiation

The spectra recorded with the three detector systems are shown in figure 2.4. Gamma-rays from 20 different isotopes were identified in these spectra, with 9 major peaks in the NaI spectrum. Of these, the most prominent is the 1596keV peak due to ^{140}La γ-rays, this isotope and its longer lived Ba parent also contribute γ-rays to several other peaks. Other NaI peaks composed largely of γ-rays from one radioisotope are the 666keV and 1392keV peaks due to ^{132}I, the 228keV peak due to ^{132}Te, and the 366keV peak due to ^{131}I. Other peaks include the 942keV peak which is composed of ^{132}I and ^{140}La γ-rays and the 144keV peak which is composed largely of ^{99m}Tc γ-rays with a ^{141}Ce component. Table 2.7 lists the principal γ-rays observed with the Ge detectors, and table 2.8 lists the major peaks in the NaI spectrum with the approximate contributions of different radionuclides.

Spectra recorded 2 weeks after irradiation

The spectra recorded with the three detector systems are shown in figure 2.5. Gamma-rays from 19 different isotopes were identified in these spectra, with 9 major peaks in the NaI spectrum. Of these, the most prominent is still the 1596keV peak due to ^{140}La. Other NaI peaks composed largely of γ-rays from one radioisotope are the 228keV peak due to ^{132}Te, and the 684keV and 1128keV peaks due to ^{132}I. In addition to these, the 348keV peak is due largely to ^{131}I and ^{140}La, the 498keV peak is due largely to ^{103}Ru and ^{140}Ba-La, the 762keV peak is due largely to ^{95}Zr-Nb and ^{140}La and the peak at 936keV is largely due to ^{132}I and ^{140}La. It is possible to strip out the components due to ^{140}La-Ba from these peaks using the 1596keV peak. Table 2.9 lists the principal γ-rays observed with the Ge detectors, and table 2.10 lists the major peaks in the NaI spectrum with the approximate contributions of different radionuclides.

Spectra recorded 1 month after irradiation

The spectra recorded with the three detector systems are shown in figure 2.6. Gamma-rays from 18 different isotopes were identified in these spectra, including ^{137}Cs which is resolved in the Ge detectors for the first time at this stage, and there are only 6 major peaks in the NaI spectrum. Of these, the most prominent is still the 1596keV peak due to ^{140}La, as is 930keV peak. Other NaI peaks include the 138keV peak due largely to ^{144}Ce and ^{147}Nd, the 336keV peak due to ^{131}I and ^{140}Ba-La, the 462keV peak due largely to ^{103}Ru and ^{140}Ba-La, and the 756keV peak is due largely to ^{95}Zr-Nb and ^{140}La. Again, it is possible to strip out the components due to ^{140}La-Ba form these peaks using the 1596keV peak. Table 2.11 lists the principal γ-rays observed with the Ge detectors, and table 2.12 lists the major peaks in the NaI spectrum with the approximate

contributions of different radionuclides.

Spectra recorded 2 months after irradiation

The spectra recorded using the three detector systems are shown in figure 2.7. Gamma-rays from 15 different isotopes were identified in these spectra, with 5 major peaks in the NaI spectrum. Of these, the most prominent is still the 1596keV peak due to ^{140}La. The other prominent peaks in the NaI spectrum are the 498keV peak due to ^{103}Ru and ^{140}Ba-La, and the 756 keV peak due largely to ^{95}Zr-Nb. Table 2.14 lists the principal γ-rays observed with the Ge detectors, and table 2.15 lists the major peaks in the NaI spectrum with the approximate contributions of different radionuclides.

Spectra recorded 6 months after irradiation

The spectra recorded using the three detector systems are shown in figure 2.8. The lower threshold on the NaI detector had been increased during a survey to reduce dead-time due to lower energy scattered γ-rays, and had not been reduced afterwards resulting in the sharp cut-off in the NaI spectrum at about 200keV. Gamma-rays from only 7 different isotopes were identified in these spectra, with just 2 major peaks in the NaI spectrum. The 498keV peak is composed of ^{103}Ru γ-rays, and the 750keV peak is due to ^{95}Zr-Nb γ-rays. A shoulder on the low energy side of the 750keV peak is from ^{137}Cs γ-rays, although this is not fully resolved it is possible to measure ^{137}Cs deposition using this shoulder. Table 2.15 lists the principal γ-rays observed with the Ge detectors, and table 2.16 lists the major peaks in the NaI spectrum with the approximate contributions of different radionuclides.

Spectra recorded 11 months after irradiation

The last set of spectra recorded using the three detector systems are shown in figure 2.9. Gamma-rays from only 5 different isotopes were identified in these spectra. The only major peak is the 750keV peak due to ^{95}Zr-Nb γ-rays, with the ^{137}Cs shoulder. Table 2.17 lists the principal γ-rays observed with the Ge detectors, and table 2.18 lists the only major peak in the NaI spectrum with the approximate contributions of different radionuclides.

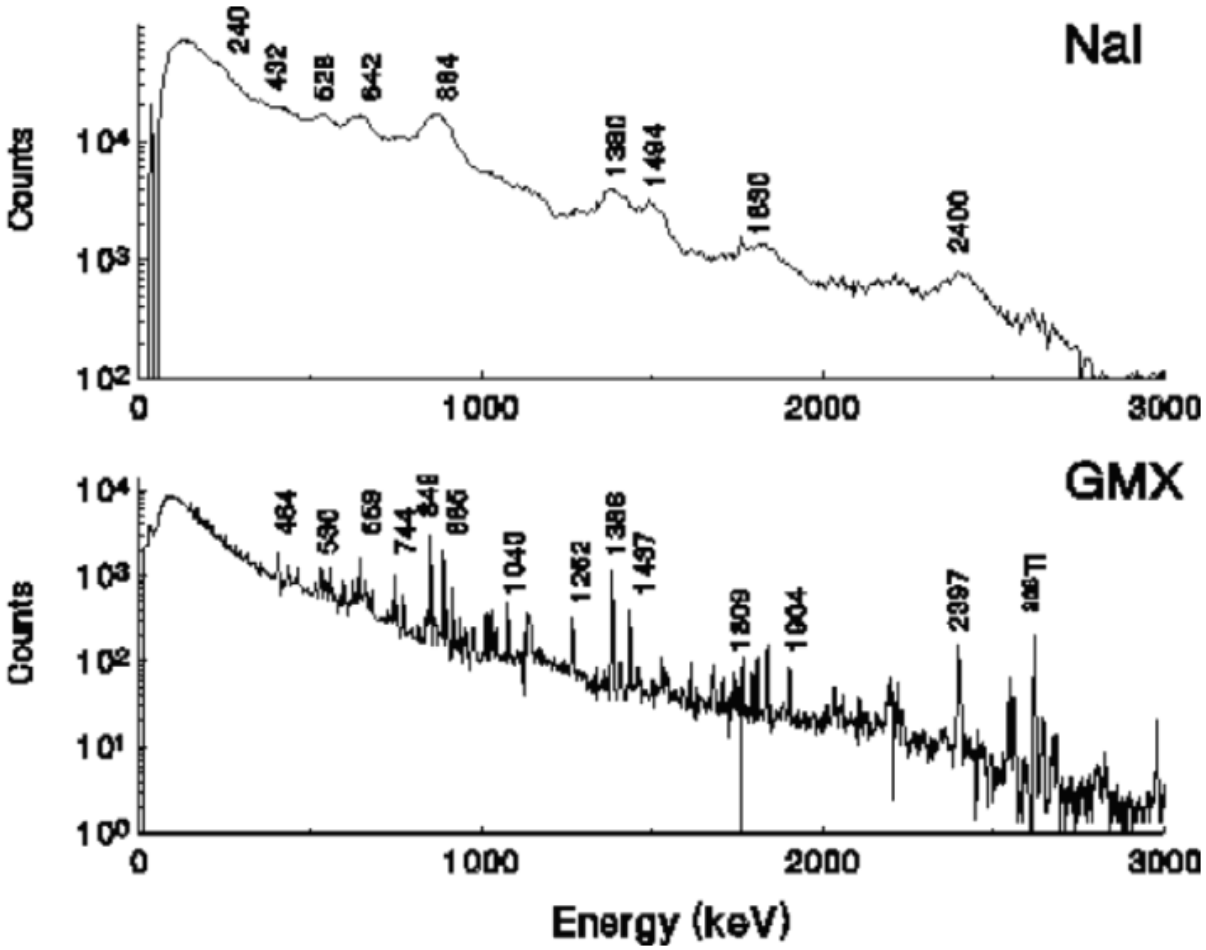

Figure 2.1: Background subtracted spectra produced by the summation of spectra recorded with the NaI and GMX detector systems **3 hours** after irradiation. The total livetime for the NaI detector was 1200s, and for the GMX detector 2000s. Approximate energies for some of the peaks are shown, with energies of the principal γ-rays observed in the GMX spectrum given in table 2.1, and the compositions of the peaks in the NaI spectrum given in table 2.2.

γ-ray energy (keV)	Nuclide	Half life	γ-ray energy (keV)	Nuclide	Half life
196.3	^{88}Kr	2.84h	847.0	^{134}I	52.60m
210.5	^{134}Te	41.83m	884.1	^{134}I	52.60m
249.8	^{135}Xe	9.09h	912.7,914.8	^{133m}Te	55.40m
402.6	^{87}Kr	1.27h	1009.8	^{138}Cs	32.20m
405.5	^{134}I	52.60m	1024.3	^{91}Sr	9.52h
435.1	^{134}Te	41.83m	1038.8	^{135}I	20.80h
462.8	^{138}Cs	32.20m	1040.3	^{134}I	52.60m
529.9	^{133}I	20.80h	1072.6	^{134}I	52.60m
555.6	^{91m}Y	(9.52h)	1131.5	^{135}I	6.61h
641.3	^{142}La	1.52h	1260.4	^{135}I	6.61h
657.9	^{97}Nb	(16.90h)	1383.9	^{92}Sr	2.71h
742.6	^{134}Te	41.83m	1435.9	^{138}Cs	32.20m
743.4	^{97m}Nb	(16.90h)	1806.8	^{134}I	52.60m
765.8	^{95}Nb	(63.98d)	1836	^{88}Rb	17.80m
767.2	^{134}Te	41.83m	1901.3	^{142}La	1.52h
			2397.8	^{142}La	1.52h

Table 2.1: Principal γ-rays observed in the GMX spectrum recorded **3 hours** after irradiation.

Peak Energy (keV)	Composition
240	^{88}Kr 30%, ^{135}Xe 20%, ^{134}Te 15%
432	^{134}I 30%, ^{134}Te 25%, ^{87}Kr 25%
528	^{133}I 30%, ^{91m}Y 25%, ^{134}I 20%, ^{138}Cs 10%
642	^{142}La 40%, ^{134}I 30%, ^{97}Nb 15%
864	^{134}I 80%, ^{133m}Te 10%
1380	^{92}Sr 75%, ^{138}Cs 25%
1494	^{135}I 40%, ^{88}Kr 35%
1830	^{88}Rb 45%, ^{134}I 30%, ^{135}I 20%
2400	^{88}Kr 55%, ^{142}La 45%

Table 2.2: The approximate contributions of radioisotopes to the major net peaks in the NaI spectrum recorded **3 hours** after irradiation, determined from the spectrum recorded at the same time using the GMX detector.

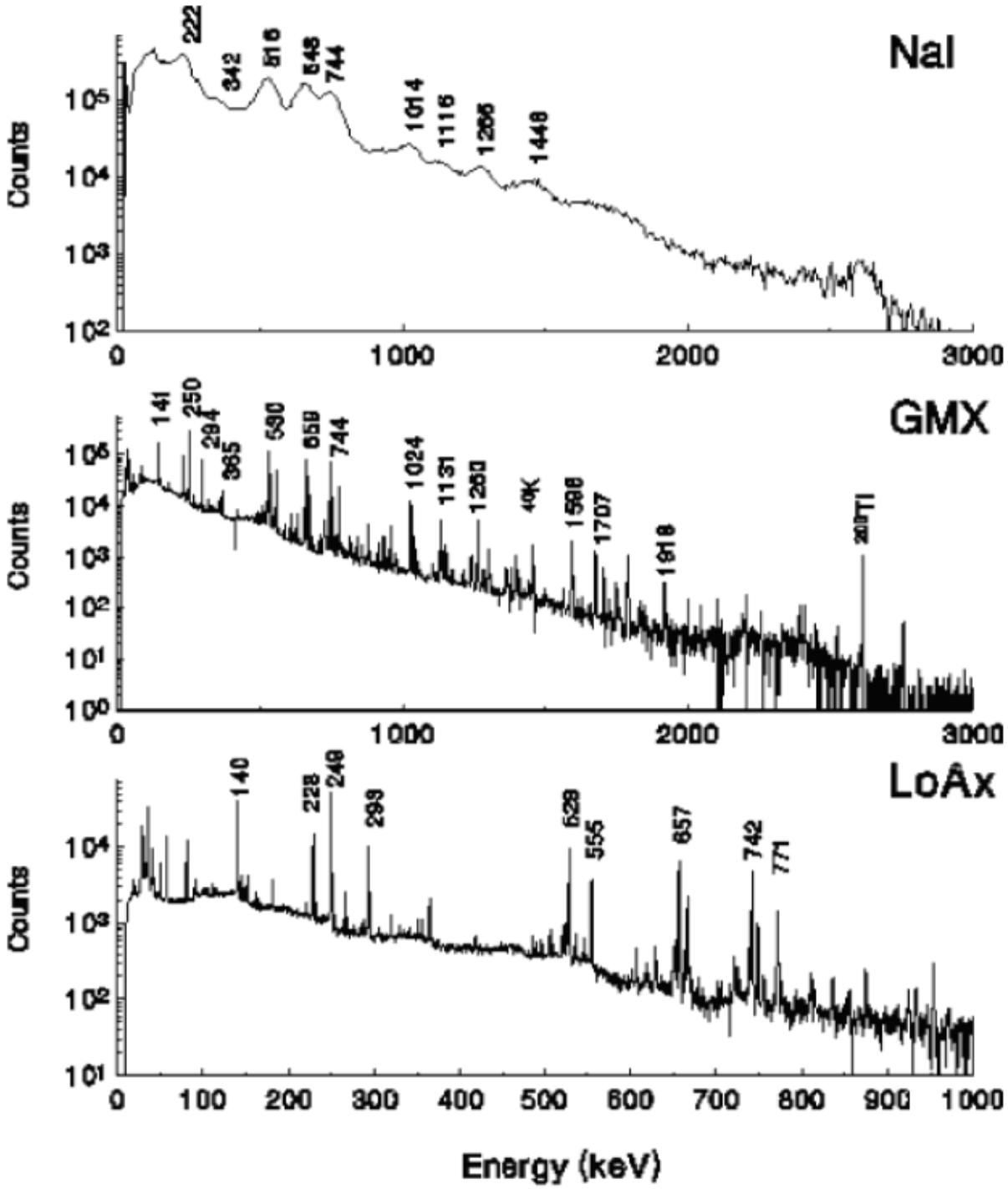

Figure 2.2: Background subtracted spectra produced by the summation of spectra recorded with the three detector systems **1 day** after irradiation. The total livetimes for all three detectors were 6000s. Approximate energies for some of the peaks are shown, with energies of the principal γ-rays observed in the Ge spectra given in table 2.3, and the composition of the peaks in the NaI spectrum given in table 2.4.

γ-ray energy (keV)	Nuclide	Half life	γ-ray energy (keV)	Nuclide	Half life
81	^{133}Xe	5.25d	836.8	^{135}I	6.61h
140.5	^{99m}Tc, ^{99}Mo	(2.75d)	875.3	^{133}I	20.80h
228.2	^{132}Te	3.26d	954.6	^{132}I	(3.26d)
249.8	^{135}Xe	9.09h	1024.3	^{91}Sr	9.52h
293.3	^{143}Ce	1.38d	1038.8	^{135}I	6.61h
364.5	^{131}I	8.04d	1125.5	^{131m}Te	1.25d
529.9	^{133}I	20.80h	1131.5	^{135}I	6.61h
555.6	^{91m}Y	(9.52h)	1260.4	^{135}I	6.61h
657.9	^{97}Nb	(16.90h)	1457.6	^{135}I	6.61h
667.7	^{132}I	(3.26d)	1596.2	^{140}La	(12.74d)
743.4	^{97m}Nb	(16.90h)	1706.5	^{135}I	6.61h
772.6	^{132}I	(3.26d)	1791.2	^{135}I	6.61h
815.8	^{140}La	(12.74d)	1917.8	^{93}Y	10.10h

Table 2.3: Principal γ-rays observed in the spectra recorded using the Ge detectors **1 day** after irradiation.

Peak Energy (keV)	Composition
222	^{135}Xe 75%, ^{132}Te 20%
342	^{131}I 45%, ^{143}Ce 20%, ^{105}Rh 12%
516	^{133}I 60%, ^{91m}Y 25%, ^{97}Zr 5%
648	^{97}Nb 65%, ^{132}I 20%, ^{91}Sr 5%
744	^{97m}Nb 55%, ^{132}I 15%, ^{91}Sr 10%
1014	^{91}Sr 85%, ^{135}I 13%
1116	^{135}I 60%, ^{131m}Te 20%, ^{97}Zr 10%
1266	^{135}I 70%, ^{133}I 25%
1446	^{135}I 70%, ^{91}Sr 15%

Table 2.4: The approximate contributions of radioisotopes to the major peaks in the NaI spectrum recorded **1 day** after irradiation, determined from the spectra recorded at the same time using the Ge detectors.

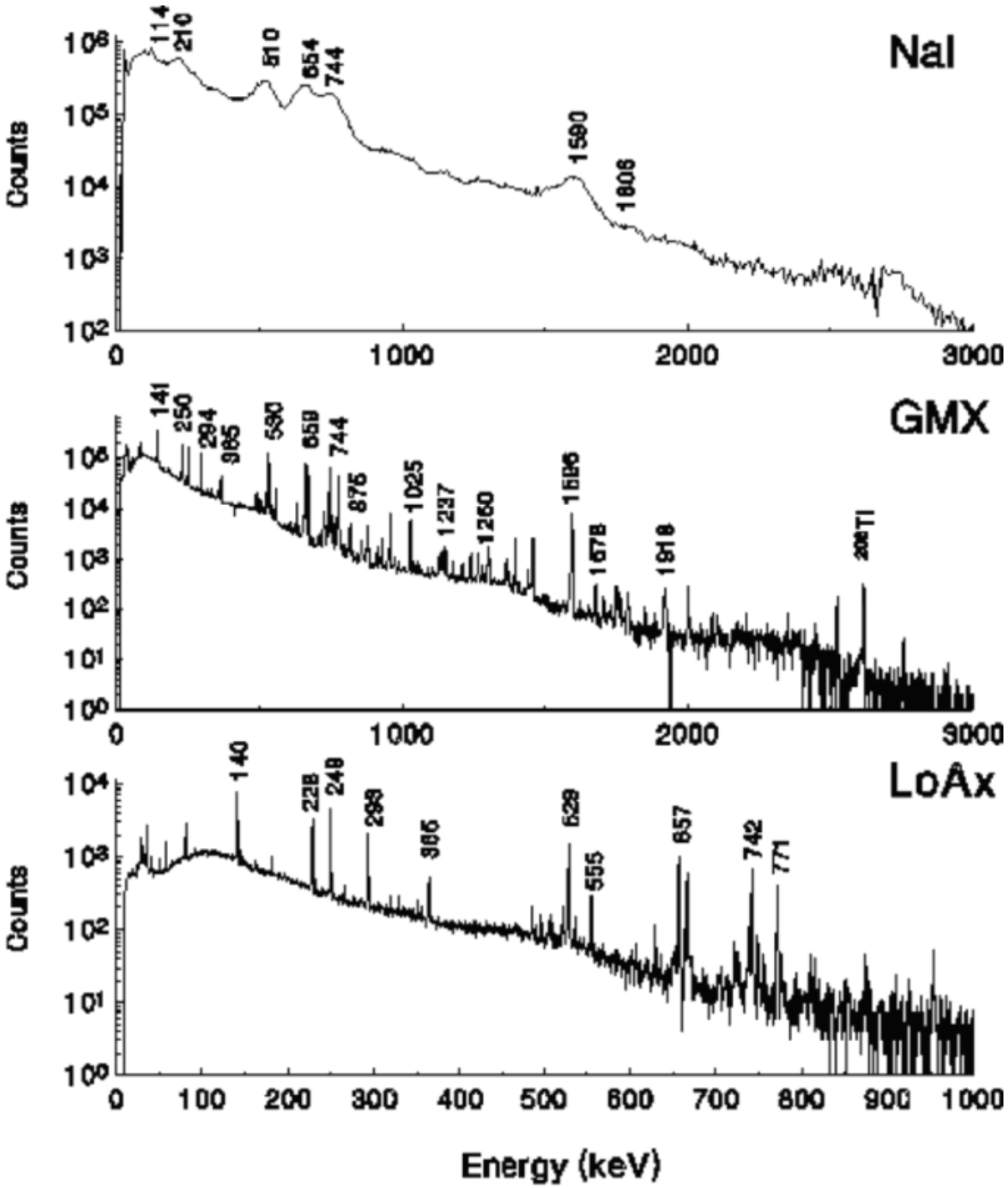

Figure 2.3: Background subtracted spectra produced by the summation of spectra recorded with the three detector systems **2 days** after irradiation. The total livetime for the NaI detector was 6000s, 3000s for the GMX detector and 1000s for the LoAx. Approximate energies for some of the peaks are shown, with energies of the principal γ-rays observed in the Ge spectra given in table 2.5, and the composition of the peaks in the NaI spectrum given in table 2.6.

γ-ray energy (keV)	Nuclide	Half life	γ-ray energy (keV)	Nuclide	Half life
81	^{133}Xe	5.25d	743.4	^{97m}Nb	(16.90h)
140.5	^{99m}Tc, ^{99}Mo	(2.75d)	772.6	^{132}I	(3.26d)
228.2	^{132}Te	3.26d	875.3	^{133}I	20.80h
249.8	^{135}Xe	9.09h	954.6	^{132}I	(3.26d)
293.3	^{143}Ce	1.38d	1024.3	^{91}Sr	9.52h
318.9	^{105}Rh	1.47d	1236.4	^{133}I	20.80h
328.8	^{140}La	(12.74d)	1260.4	^{135}I	6.61h
364.5	^{131}I	8.04d	1298.2	^{133}I	20.80h
487.0	^{140}La	(12.74d)	1398.7	^{132}I	(3.26d)
529.9	^{133}I	20.80h	1596.2	^{140}La	(12.74d)
537.3	^{140}Ba	12.74d	1678	^{135}I	6.61h
555.6	^{91m}Y	(9.52h)	1791.2	^{135}I	6.61h
630.2	^{132}I	(3.26d)	1917.8	^{93}Y	10.10h
657.9	^{97}Nb	(16.90h)	1921.1	^{132}I	(3.26d)
667.7	^{132}I	(3.26d)	2002.3	^{132}I	(3.26d)
722.0	^{143}Ce	1.38d	2521.3	^{140}La	(12.74d)

Table 2.5: Principal γ-rays observed in spectra recorded using the Ge detectors **2 days** after irradiation.

Peak Energy (keV)	Composition
114	^{99m}Tc ^{99}Mo 70%, ^{133}Xe 20%
210	^{135}Xe 50%, ^{132}Te 45%
510	^{133}I 50%, ^{132}I 10%, ^{91m}Y 10%, ^{140}La 10%
654	^{132}I 45%, ^{97}Nb 45%
744	^{97m}Nb 45% , ^{132}I 35%, ^{143}Ce 5%
1590	^{140}La 95%, ^{135}I 5%
1806	^{135}I 70%, ^{97}Zr 25%

Table 2.6: The approximate contributions of radioisotopes to the major peaks in the NaI spectrum recorded **2 days** after irradiation, determined from the spectra recorded at the same time using the Ge detectors.

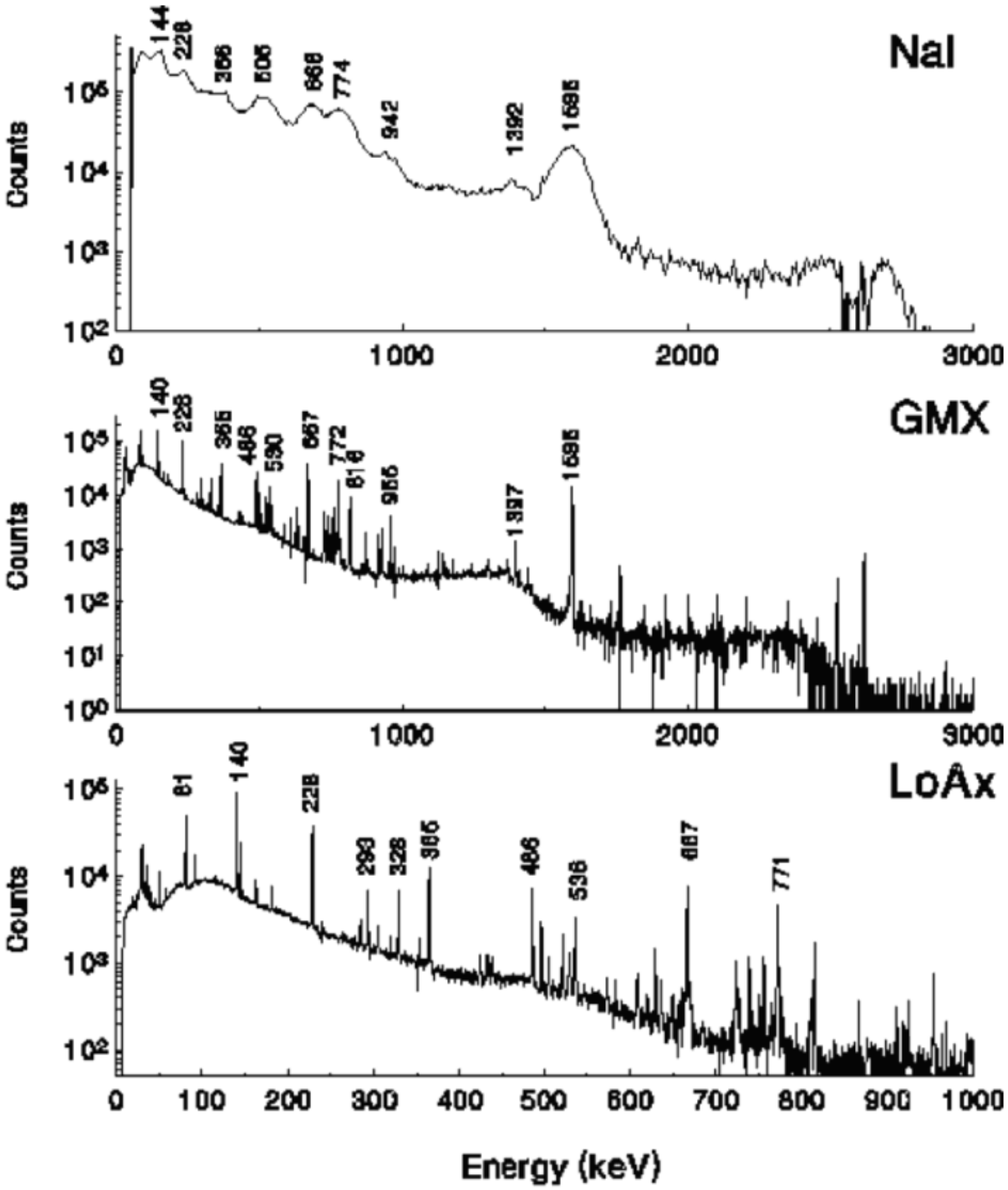

Figure 2.4: Background subtracted spectra produced by the summation of spectra recorded with the three detector systems **7 days** after irradiation. The total livetimes for both Ge detectors were 40000s, the livetime for the NaI detector was 6000s. Approximate energies for some of the peaks are shown, with energies for the principal γ-rays observed in the Ge spectra given in table 2.7, and the compositions of the peaks in the NaI spectrum given in table 2.8.

γ-ray energy (keV)	Nuclide	Half life	γ-ray energy (keV)	Nuclide	Half life
81	^{133}Xe	5.25d	667.7	^{132}I	(3.26d)
91.1	^{147}Nd	10.98d	724.2	^{95}Zr	63.98d
140.5	^{99m}Tc, ^{99}Mo	(2.75d)	739.5	^{99}Mo	2.75d
145.4	^{141}Ce	32.50d	756.7	^{95}Zr	63.98d
162.6	^{140}Ba	12.74d	772.6	^{132}I	(3.26d)
181.1	^{99}Mo	2.75d	815.8	^{140}La	(12.74d)
228.2	^{132}Te	3.26d	867.8	^{140}La	(12.74d)
284.3	^{131}I	8.04d	925.2	^{140}La	(12.74d)
293.3	^{143}Ce	1.38d	954.6	^{132}I	(3.26d)
364.5	^{131}I	8.04d	1136.0	^{132}I	(3.26d)
487.0	^{140}La	(12.74d)	1295.3	^{132}I	(3.26d)
497.1	^{103}Ru	39.35d	1398.7	^{132}I	(3.26d)
522.7	^{132}I	(3.26d)	1596.2	^{140}La	(12.74d)
531.0	^{147}Nd	10.98d	1921.1	^{132}I	(3.26d)
537.3	^{140}Ba	12.74d	2521.3	^{140}La	(12.74d)
630.2	^{132}I	(3.26d)			

Table 2.7: Principal γ-rays observed in spectra recorded using the Ge detectors **7 days** after irradiation.

Peak Energy (keV)	Composition
144	^{99m}Tc ^{99}Mo 70%, ^{141}Ce 20%
228	^{132}Te 95%
366	^{131}I 90%, ^{143}Ce 7%
505	^{140}La ^{140}Ba 50%, ^{132}I 20%, ^{103}Ru 15%
666	^{132}I 95%
774	^{132}I 45%, ^{95}Zr 20%, ^{140}La 15%, ^{99}Mo 10%
942	^{132}I 60%, ^{140}La 30%
1392	^{132}I
1596	^{140}La

Table 2.8: The approximate contributions of radioisotopes to the major peaks in the NaI spectrum recorded **7 days** after irradiation, determined from the spectra recorded at the same time using the Ge detectors.

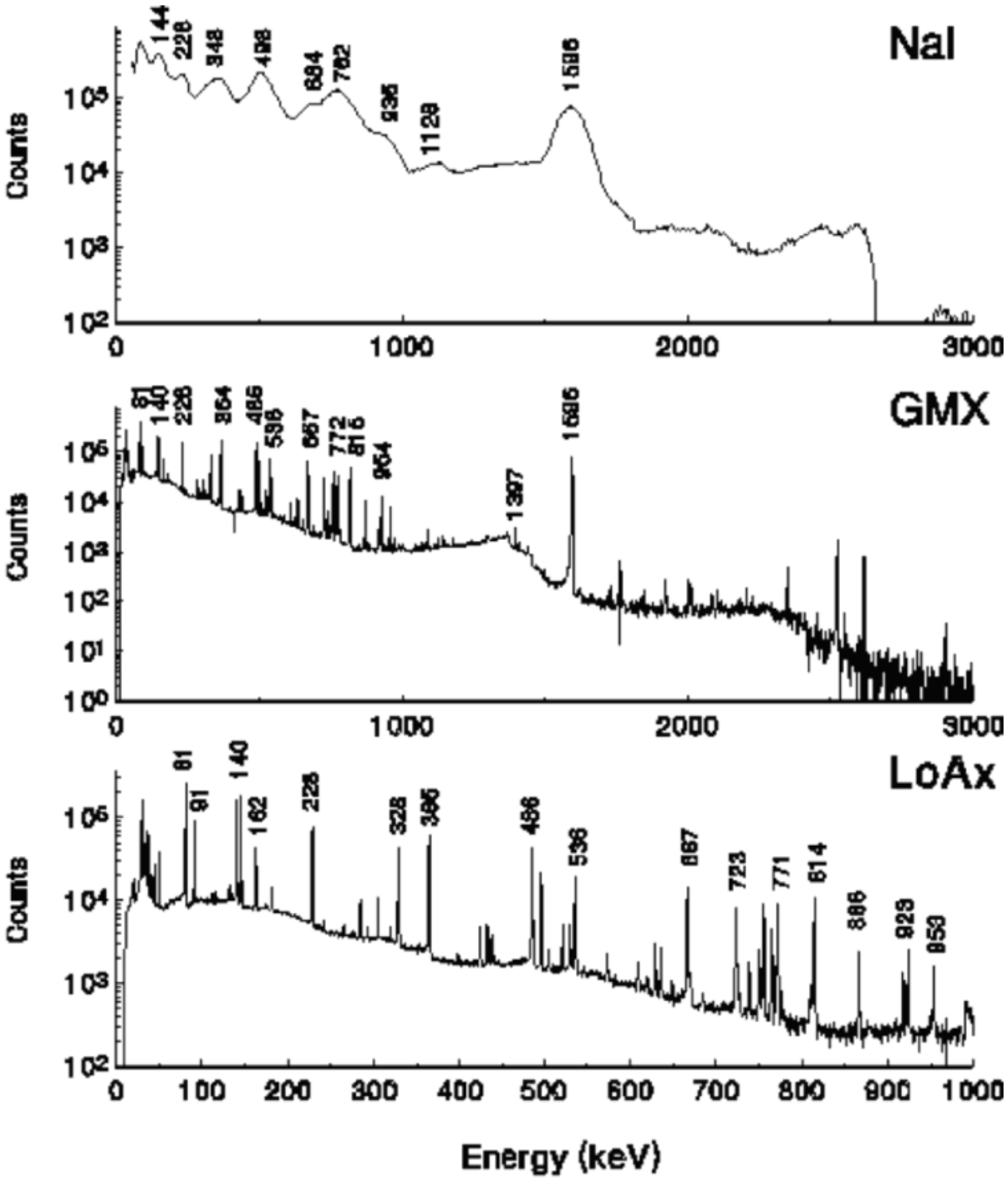

Figure 2.5: Background subtracted spectra produced by the summation of spectra recorded with the three detector systems **14 days** after irradiation. The total livetimes for both Ge detectors were 40000s, the livetime for the NaI detector was 6000s. Approximate energies for some of the peaks are shown, with energies of the principal γ-rays observed in the Ge spectra given in table 2.9, and the compositions of the peaks in the NaI spectrum given in table 2.10.

γ-ray energy (keV)	Nuclide	Half life	γ-ray energy (keV)	Nuclide	Half life
81	^{133}Xe	5.25d	531.0	^{147}Nd	10.98d
91.1	^{147}Nd	10.98d	537.3	^{140}Ba	12.74d
140.5	^{99m}Tc, ^{99}Mo	(2.75d)	630.2	^{132}I	(3.26d)
145.4	^{141}Ce	32.50d	637.0	^{131}I	8.04d
162.6	^{140}Ba	12.74d	667.7	^{132}I	(3.26d)
181.1	^{99}Mo	2.75d	724.2	^{95}Zr	63.98d
228.2	^{132}Te	3.26d	756.7	^{95}Zr	63.98d
284.3	^{131}I	8.04d	765.8	^{95}Nb	(63.98d)
304.9	^{140}Ba	12.74d	772.6	^{132}I	(3.26d)
328.8	^{140}La	(12.74d)	815.8	^{140}La	(12.74d)
364.5	^{131}I	8.04d	867.8	^{140}La	(12.74d)
423.7	^{140}Ba	12.74d	925.2	^{140}La	(12.74d)
431.9	^{132}I	(3.26d)	954.6	^{132}I	(3.26d)
487.0	^{140}La	(12.74d)	1398.7	^{132}I	(3.26d)
497.1	^{103}Ru	39.35d	1596.2	^{140}La	(12.74d)
522.7	^{132}I	(3.26d)	2347.8	^{140}La	(12.74d)
			2521.3	^{140}La	(12.74d)

Table 2.9: Principal γ-rays measured in spectra recorded using the Ge detectors **2 weeks** after irradiation.

Peak Energy (keV)	Composition
144	^{141}Ce 50%, ^{99m}Tc ^{99}Mo 45%
228	^{132}Te 95%
348	^{131}I 60%, ^{140}La 35%
498	^{140}La ^{140}Ba 70%, ^{103}Ru 20%, ^{132}I 5%
684	^{132}I
762	^{95}Zr ^{95}Nb 45%, ^{140}La 30%, ^{132}I 20%
936	^{140}La 60%, ^{132}I 35%
1128	^{132}I 85%
1596	^{140}La

Table 2.10: The approximate contributions of radionuclides to the major peaks in the NaI spectrum recorded **2 weeks** after irradiation, determined from the spectra recorded at the same time using the Ge detectors.

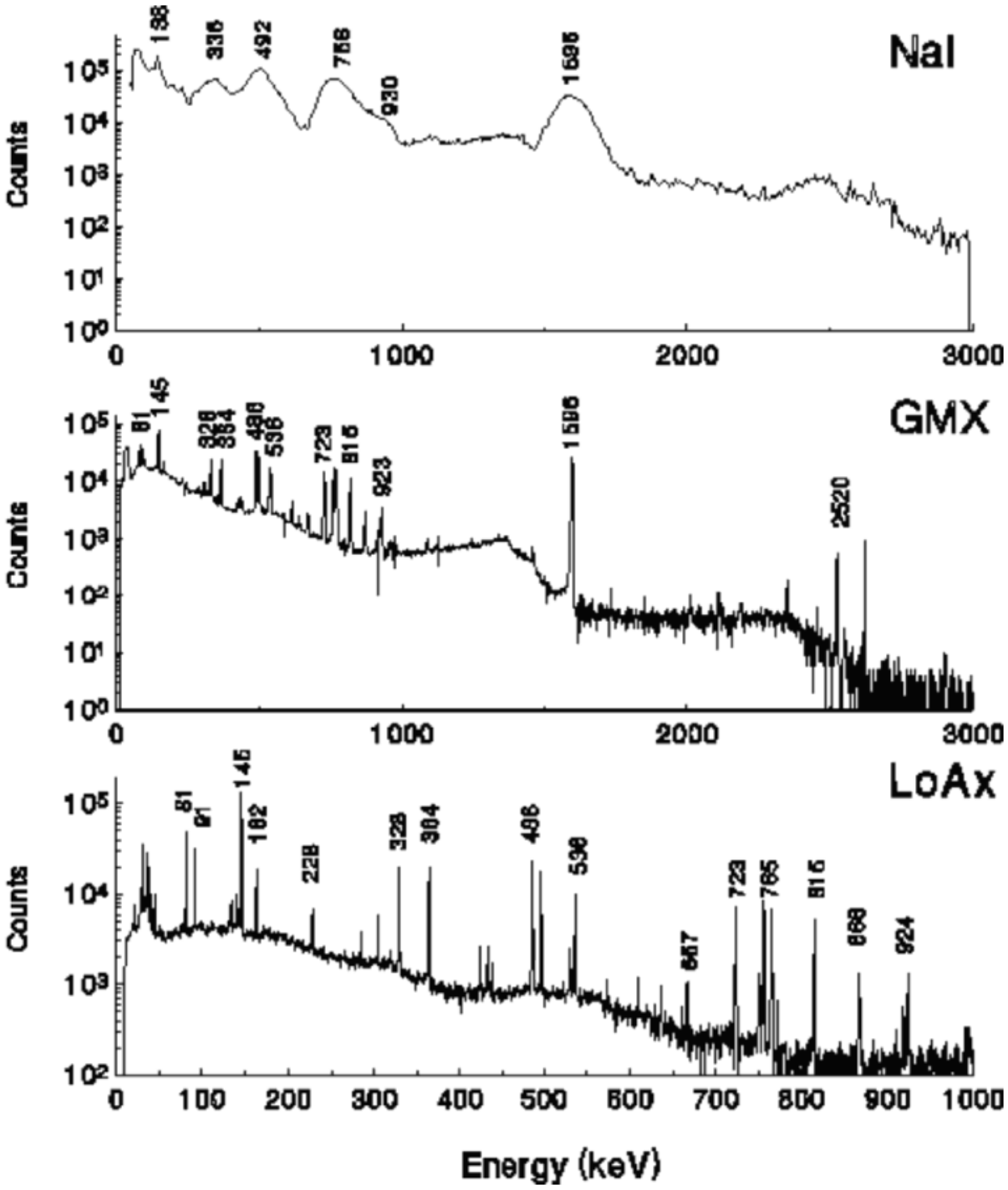

Figure 2.6: Background subtracted spectra produced by the summation of spectra recorded with the three detector systems **1 month** after irradiation. The total livetime for the NaI spectrum was 6000s, the livetimes for both Ge spectra were 40000s. Approximate energies for some of the peaks are shown, with energies of the principal γ-rays observed in the Ge spectra given in table 2.11, and the compositions of the peaks in the NaI spectrum given in table 2.12.

γ-ray energy (keV)	Nuclide	Half life	γ-ray energy (keV)	Nuclide	Half life
81	^{133}Xe	5.25d	537.3	^{140}Ba	12.74d
91.1	^{147}Nd	10.98d	610.3	^{103}Ru	39.35d
133.5	^{144}Ce	284.90d	637.0	^{131}I	8.04d
145.4	^{141}Ce	32.50d	661.6	^{137}Cs	30.00y
162.6	^{140}Ba	12.74d	667.7	^{132}I	(3.26d)
228.2	^{132}Te	3.26d	724.2	^{95}Zr	63.98d
284.3	^{131}I	8.04d	756.7	^{95}Zr	63.98d
304.9	^{140}Ba	12.74d	765.8	^{95}Nb	(63.98d)
328.8	^{140}La	(12.74d)	815.8	^{140}La	(12.74d)
364.5	^{131}I	8.04d	867.8	^{140}La	(12.74d)
423.7	^{140}Ba	12.74d	925.2	^{140}La	(12.74d)
487.0	^{140}La	(12.74d)	1596.2	^{140}La	(12.74d)
497.1	^{103}Ru	39.35d	2521.3	^{140}La	(12.74d)
531.0	^{147}Nd	10.98d			

Table 2.11: Principal γ-rays observed in spectra recorded with the Ge detectors **1 month** after irradiation.

Peak Energy (keV)	Composition
138	^{144}Ce 50%, ^{147}Nd 50%
336	^{140}Ba ^{140}La 55%, ^{131}I 45%
492	^{140}Ba ^{140}La 60%, ^{103}Ru 35%
756	^{95}Nb ^{95}Zr 80%, ^{140}La 20%
930	^{140}La
1596	^{140}La

Table 2.12: The approximate contributions of radioisotopes to the major peaks in the NaI spectrum recorded **1 month** after irradiation, determined from the spectra recorded at the same time using the Ge detectors.

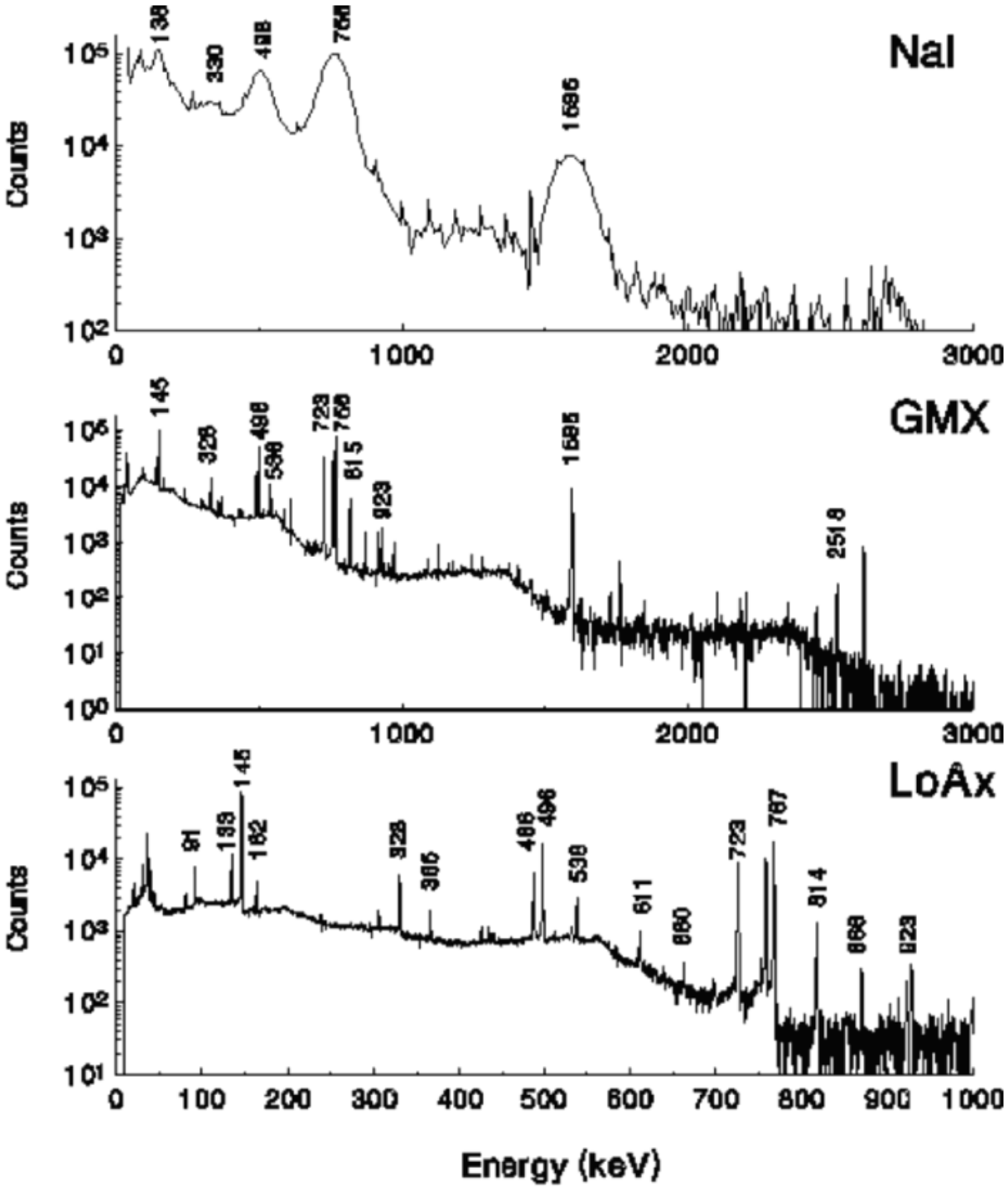

Figure 2.7: Background subtracted spectra produced by the summation of spectra recorded with the three detector systems **2 months** after irradiation. The total livetimes for the Ge detectors were 40000s, the livetime for the NaI spectrum was 6000s. Approximate energies for some of the peaks are shown, with energies of the principal γ-rays observed in the Ge spectra given in table 2.13, and the compositions of the peaks in the NaI spectrum given in table 2.14.

γ-ray energy (keV)	Nuclide	Half life	γ-ray energy (keV)	Nuclide	Half life
91.1	^{147}Nd	10.98d	661.6	^{137}Cs	30.00y
133.5	^{144}Ce	284.90d	724.2	^{95}Zr	63.98d
145.4	^{141}Ce	32.50d	756.7	^{95}Zr	63.98d
162.6	^{140}Ba	12.74d	765.8	^{95}Nb	(63.98d)
328.8	^{140}La	(12.74d)	815.8	^{140}La	(12.74d)
364.5	^{131}I	8.04d	867.8	^{140}La	(12.74d)
487.0	^{140}La	(12.74d)	925.2	^{140}La	(12.74d)
497.1	^{103}Ru	39.35d	1596.2	^{140}La	(12.74d)
537.3	^{140}Ba	12.74d	2521.3	^{140}La	(12.74d)
610.3	^{103}Ru	39.35d			

Table 2.13: Principal γ-rays observed in spectra recorded with the Ge detectors **2 months** after irradiation.

Peak Energy (keV)	Composition
138	^{141}Ce 85%, ^{140}Ba 15%
330	^{140}Ba
498	^{103}Ru 50%, ^{140}La ^{140}Ba 45%
756	^{95}Zr ^{95}Nb 97%, ^{140}La 3%
1596	^{140}La

Table 2.14: The approximate contributions of radioisotopes to the major peaks in the NaI spectrum recorded **2 months** after irradiation, determined from the spectra recorded at the same time using the Ge detectors.

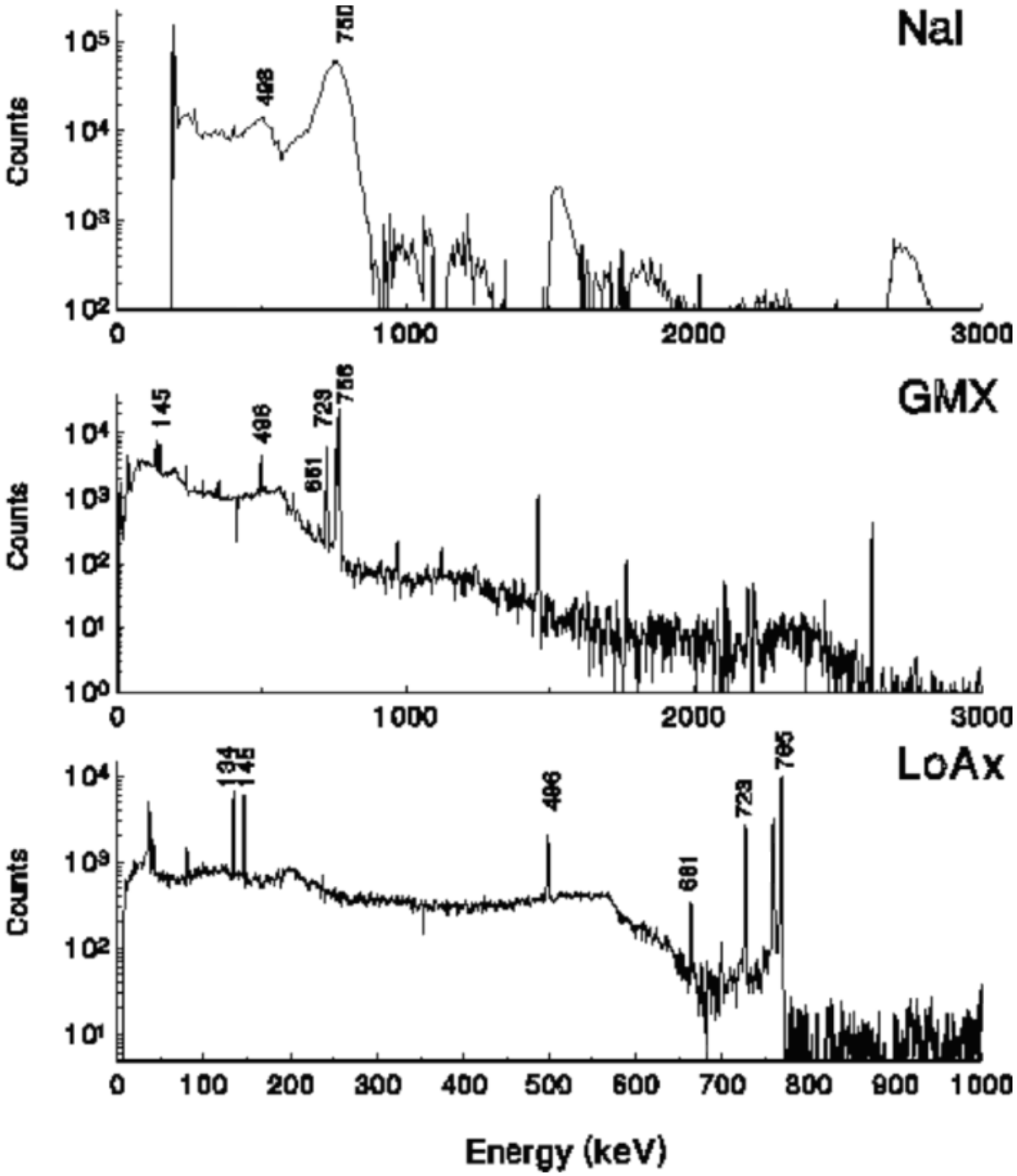

Figure 2.8: Background subtracted spectra produced by the summation of spectra recorded with the three detector systems **6 months** after irradiation. The total livetimes for the Ge detectors were 40000s, and for the NaI detector 6000s. Approximate energies for some of the peaks are shown, with energies for the principal γ-rays observed in the Ge spectra given in table 2.15, and the compositions of the peaks in the NaI spectrum given in table 2.16.

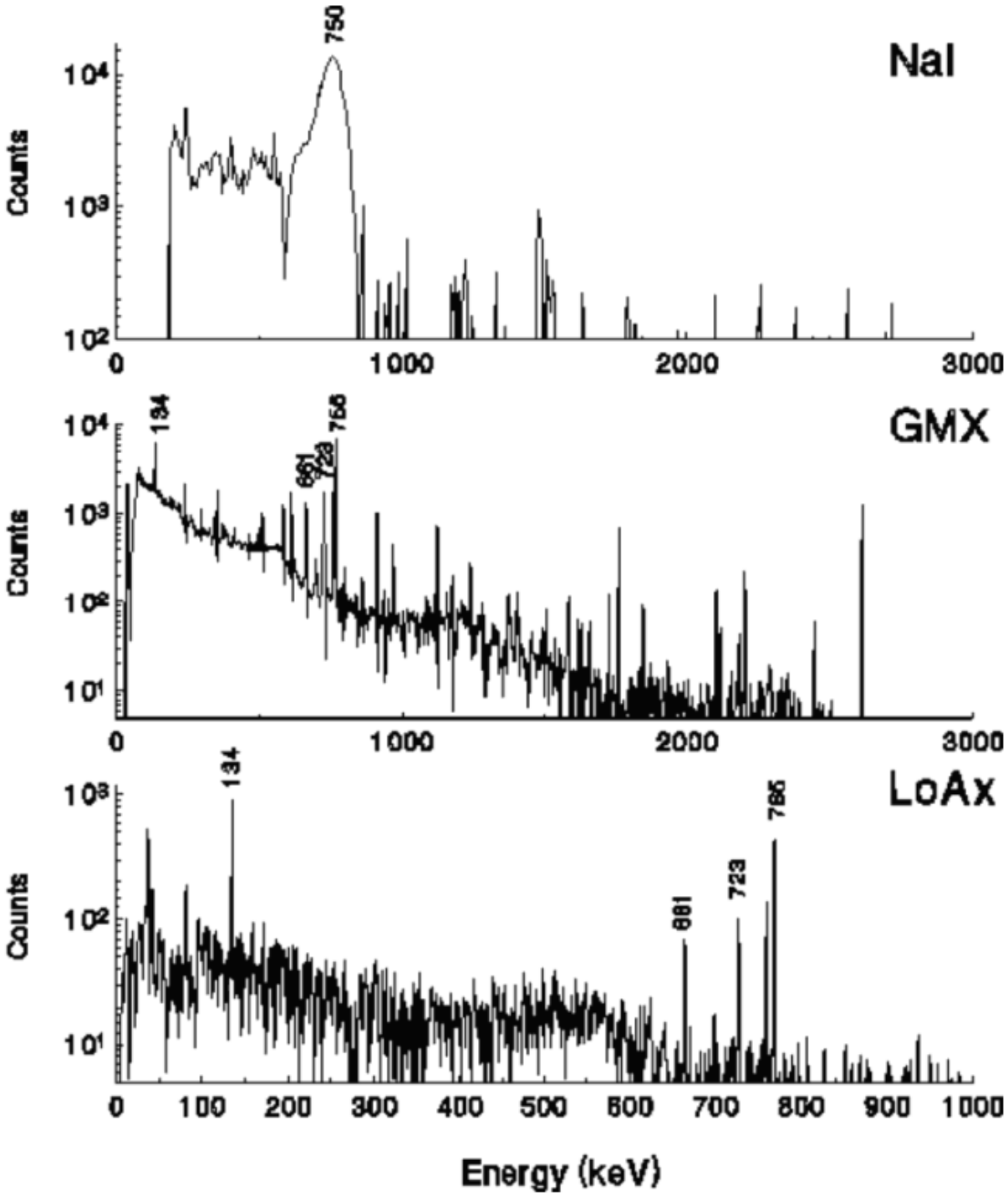

Figure 2.9: Background subtracted spectra produced by the summation of spectra recorded with the three detector systems **11 months** after irradiation. The total livetimes for the Ge detectors were 40000s, and 6000s for the NaI detector. Approximate energies for some of the peaks are shown, with energies for the principal γ-rays observed in the Ge spectra given in table 2.17, and the composition of the peaks in the NaI spectrum given in table 2.18.

γ-ray energy (keV)	Nuclide	Half life	γ-ray energy (keV)	Nuclide	Half life
91.1	^{147}Nd	10.98d	661.6	^{137}Cs	30.00y
133.5	^{144}Ce	284.90d	724.2	^{95}Zr	63.98d
145.4	^{141}Ce	32.50d	756.7	^{95}Zr	63.98d
497.1	^{103}Ru	39.35d	765.8	^{95}Nb	(63.98d)

Table 2.15: Principal γ-rays observed in spectra recorded with the Ge detectors **6 months** after irradiation.

Peak Energy (keV)	Composition
498	^{103}Ru
750	^{95}Zr ^{95}Nb

Table 2.16: The approximate contributions of radioisotopes to the major peaks in the NaI spectrum recorded **6 months** after irradiation, determined from the spectra recorded at the same time using the Ge detectors.

γ-ray energy (keV)	Nuclide	Half life	γ-ray energy (keV)	Nuclide	Half life
133.5	^{144}Ce	284.90d	756.7	^{95}Zr	63.98d
661.6	^{137}Cs	30.00y	765.8	^{95}Nb	(63.98d)
724.2	^{95}Zr	63.98d			

Table 2.17: γ-rays observed in spectra recorded with the Ge detectors **11 months** after irradiation.

Peak Energy (keV)	Composition
750	^{95}Zr ^{95}Nb 90%, ^{137}Cs 10%

Table 2.18: The approximate contributions of various radioisotopes to the major peak in the NaI spectrum recorded **11 months** after irradiation, determined from the spectra recorded at the same time using the Ge detectors.

2.7 Decay Characteristics

The composition of the peaks in the NaI spectra was verified by studying the decay of these peaks over time, and determining the half-lives of the components. This also helps determine the proportions of different components within composite peaks, and at what time in the decay the peaks approximate to being composed of one dominant component. It also helps to indicate where complex decay corrections might be needed when analysing spectra from reactor accidents.

The NaI spectra were gain matched, a background was subtracted and they were then combined into spectra with longer effective live times to increase counting statistics. A computer code was written which determined the net area of predefined peaks, found from a window around each peak and two other windows on nearby background areas. The background was determined from the mean counts in the background area and then subtracted from the gross area under the peak. This code was then run for each of the sets of measurements to give the variation of the net counts for the different peaks over time.

The net counts for each peak were plotted against time, and least squares fits to a function containing either one or two exponentials conducted. Figures 2.10-2.15 show the net counts and fitted curves of the peaks in the NaI spectra at various stages after irradiation. The points were fitted to functions of the form

$$A = A_1 e^{-\lambda_1 t} + A_2 e^{-\lambda_2 t} \qquad (2.1)$$

where A_1 and A_2 are constants representing the activity of each component when the sources were removed from the reactor, and λ_1 and λ_2 are the decay constants for each component. The half life and decay constants are related by $t_{½}=ln2/\lambda$. Attempts at fitting three or more exponentials resulted in very large errors in the parameters, and so were not pursued. For some sets of points only one component was significant, for others the second component was effectively constant ($\lambda_2=0$) due either to a background component or an isotope with a half life which is very long compared to the length of time over which the observations were made. Tables 2.19-2.23 give the parameters and associated half lives for the fits, along with the major components for these peaks previously determined from the corresponding Ge spectra for comparison.

The use of the double exponential function results in reasonable fits to the data points, which in some cases are widely scattered around the fitted curve. There is good agreement between the half lives of the major components of the NaI peaks identified from the Ge spectra and the half lives determined from the decay curves. These half life measurements confirm the assignments of radioisotopic contributions to the peaks in the NaI spectra, and provide valuable information on how the compositions of these peaks vary with time.

The different components are best determined from data sets recorded over a period of time that is long compared to the half lives of the components. This is especially evident in figure 2.11 and table 2.20 where only one component for each peak is distinguished. It would be possible to combine several data sets recorded with different sources or geometries, however this has not so far been attempted.

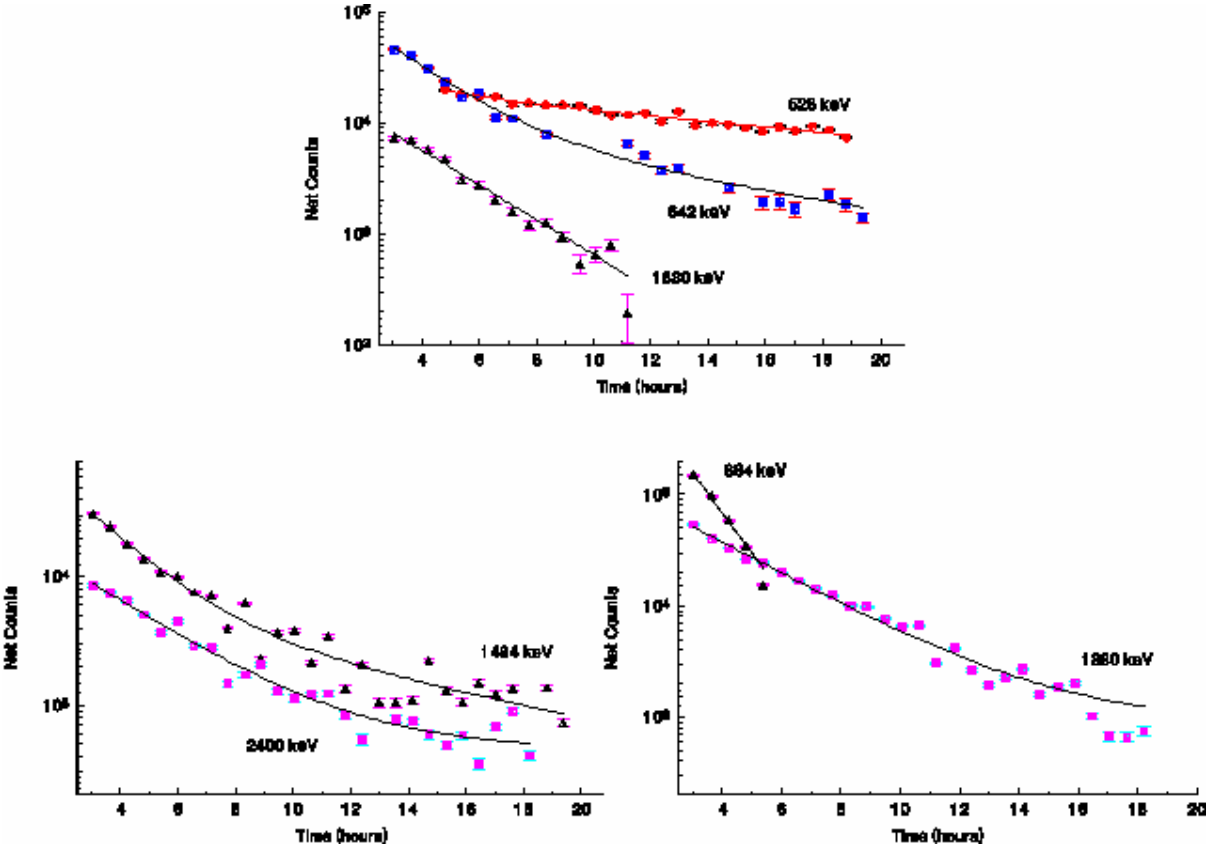

Figure 2.10: Net counts for seven peaks in the NaI spectra recorded over the first day of measurements.

Energy (keV)	Parameters				Half lives	Composition
	A_1	λ_1 (h^{-1})	A_2	λ_2 (h^{-1})		
528	58000	0.68	23000	0.058	(1.0±1.0)h (12.0±1.6)h	^{134}I (52.60m), ^{138}Cs (32.20m) ^{91m}Y (9.52h), ^{133}I (20.80h)
642	160000	0.47	11100	0.10	(1.5±0.3)h (7±5)h	^{142}La (1.52h), ^{134}I (52.60m) ^{97}Nb (16.90h)
864	1900000	0.83	-	-	(50±3)m	^{134}I (52.60m) ^{133m}Te (55.40m)
1380	135000	0.330	900	-	(2.1±0.1)h	^{92}Sr (2.71h)
1494	130000	0.53	7000	0.11	(1.3±0.2)h (6±3)h	^{88}Kr (2.84h) ^{135}I (6.61h)
1830	24000	0.36	-	-	(1.9±0.1)h	^{88}Rb (17.80m), ^{134}I (52.60m), ^{135}I (6.61h)
2400	23000	0.33	450	-	(2.1±0.1)h	^{142}La (1.52h), ^{88}Kr (2.84h)

Table 2.19: Parameters of fits to the decay curves for seven peaks in the NaI spectra recorded over the first day of measurements, with corresponding half lives and compositions from table 2.2.

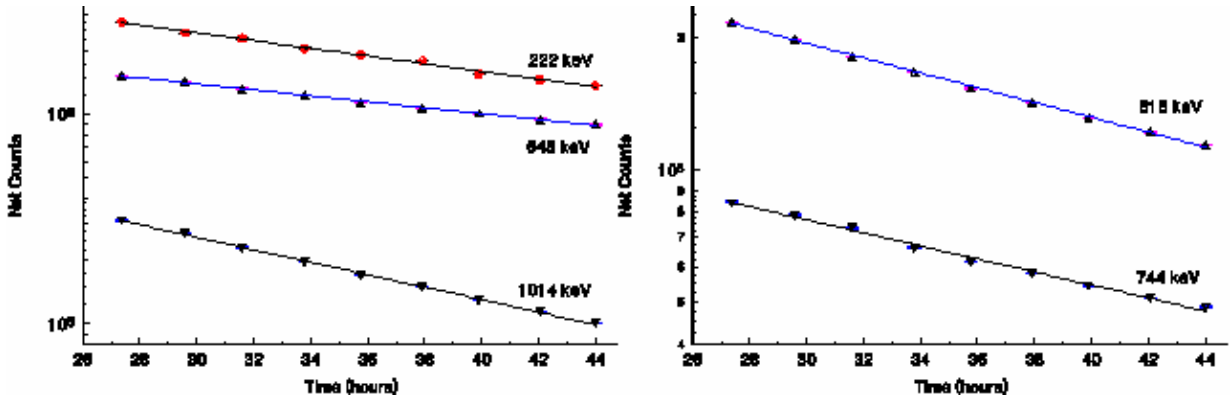

Figure 2.11: Net counts for five peaks in the NaI spectra recorded over the second day of measurements.

Energy (keV)	Parameters				Half lives	Composition
	A_1	λ_1 (h^{-1})	A_2	λ_2 (h^{-1})		
222	8600000	0.0419	-	-	(16.5±0.4)h	^{135}Xe (9.09h), ^{132}Te (3.26d)
516	6180000	0.0386	-	-	(18.0±0.3)h	^{133}I (20.80h), ^{91m}Y (9.52h)
648	3670000	0.0322	-	-	(21.5±0.3)h	^{97}Nb (16.90h), ^{132}I (3.26d)
744	2120000	0.0340	-	-	(20.4±0.6)h	^{97m}Nb (16.90h), ^{132}I (3.26d), ^{91}Sr (9.52h)
1014	1970000	0.0679	-	-	(10.2±0.1)h	^{91}Sr (9.52h), ^{135}I (6.61h)

Table 2.20: Parameters of fits to the decay curves for five peaks in the NaI spectra recorded over the second day of measurements, with corresponding half lives and compositions from table 2.4.

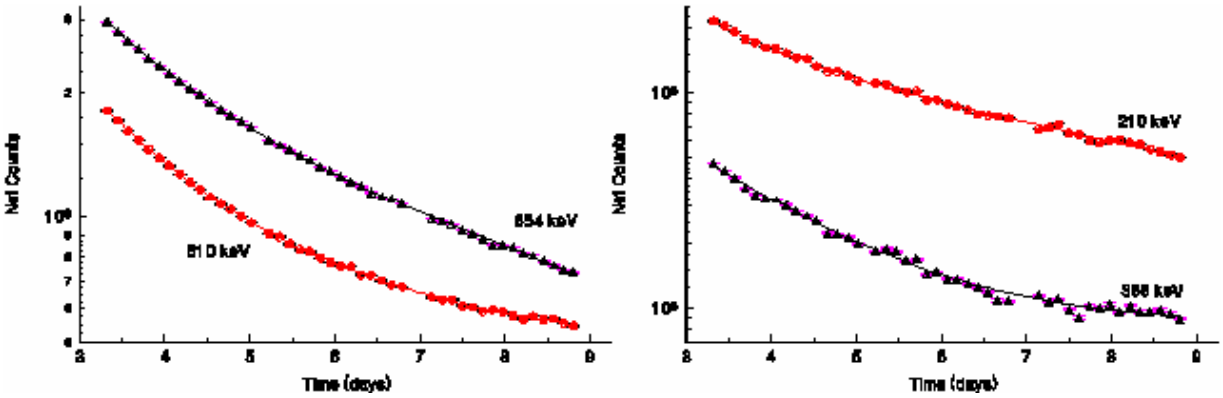

Figure 2.12: Net counts for four peaks in the NaI spectra recorded 3-9 days after irradiation.

Energy (keV)	Parameters				Half lives	Composition
	A_1	λ_1 (d^{-1})	A_2	λ_2 (d^{-1})		
210	25000000	1.09	2800000	0.192	(15±2)h (3.6±0.2)d	^{135}Xe (9.09h) ^{132}Te (3.26d)
366	3900000	0.70	83000	-	(23.8±0.7)h	^{143}Ce (1.38d) ^{131}I (8.04d)
510	11900000	0.709	800000	0.047	(23.5±0.6)h (14±2)d	^{133}I (20.80h) ^{132}I (3.26d), ^{140}La (12.74d)
654	17200000	0.80	3060000	0.165	(20.8±0.8)h (4.2±0.1)d	^{97}Nb (16.90h) ^{132}I (3.26d)

Table 2.21: Parameters of fits to the decay curves for four peaks in the NaI spectra recorded 3-9 days after irradiation, with corresponding half lives and compositions from tables 2.6 and 2.8.

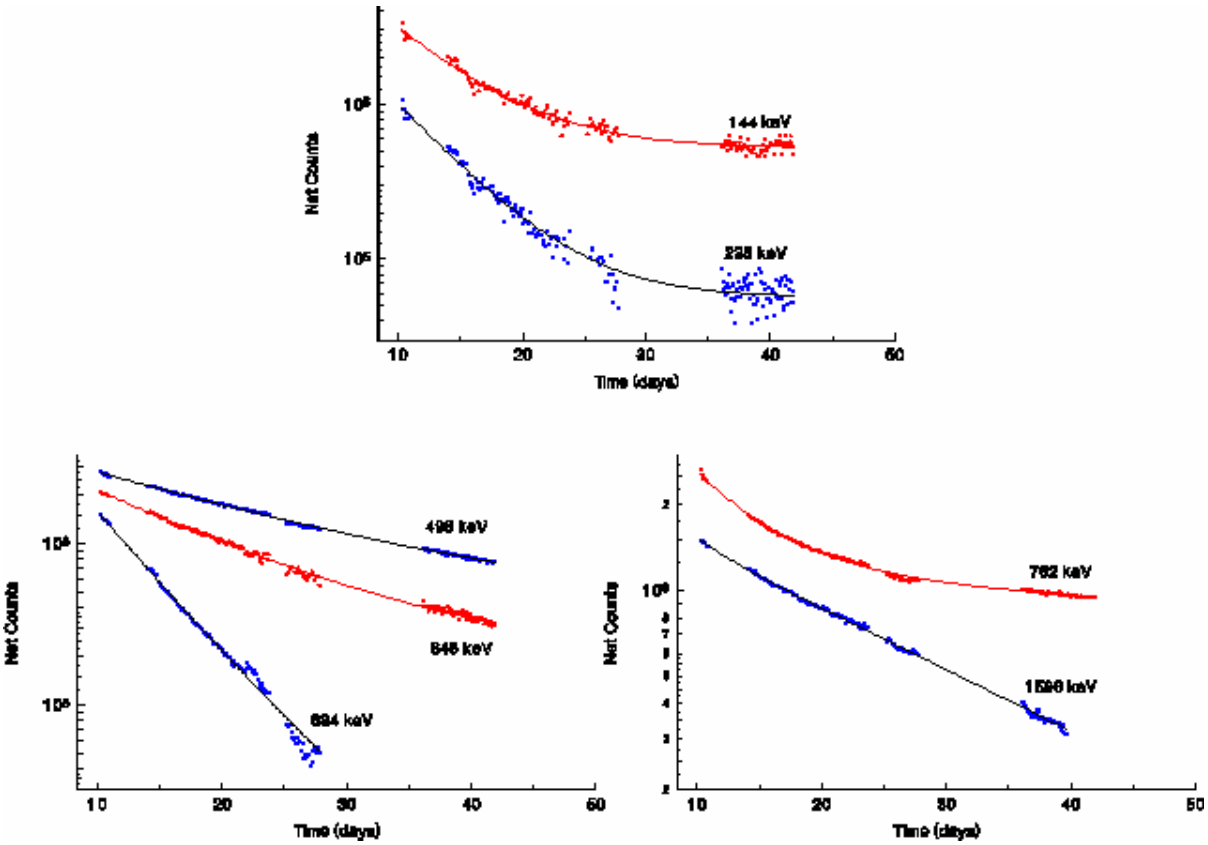

Figure 2.13: Net counts for seven peaks in the NaI spectra recorded 10-45 days after irradiation.

Energy (keV)	Parameters				Half lives	Composition
	A_1	λ_1 (d^{-1})	A_2	λ_2 (d^{-1})		
144	14200000	0.170	517000	-	(4.08±0.07)d	^{141}Ce (32.50d), ^{99m}Tc ^{99}Mo (2.75d)
228	6900000	0.199	57000	-	(3.48±0.05)d	^{132}Te (3.26d)
348	4530000	0.0851	196000	-	(8.1±0.1)d	^{131}I (8.04d), ^{140}La (12.74d)
498	4210000	0.0561	364000	-	(12.36±0.15)d	^{140}La (12.74d), ^{103}Ru (39.35d)
684	12000000	0.22	1000000	0.13	(3.2±0.7)d (5±5)d	^{132}I (3.26d)
762	8100000	0.172	1240000	0.0067	(4.03±0.09)d (103±9)d	^{140}La (12.74d), ^{132}I (3.26d) ^{95}Zr,Nb (63.98d)
1596	6000000	0.40	2320000	0.0495	(1.7±0.3)d (14.0±0.1)d	^{132}I (3.26d) ^{140}La (12.74d)

Table 2.22: Parameters of fits to the decay curves for seven peaks in the NaI spectra recorded 10-45 days after irradiation, with corresponding half lives and compositions from table 2.10.

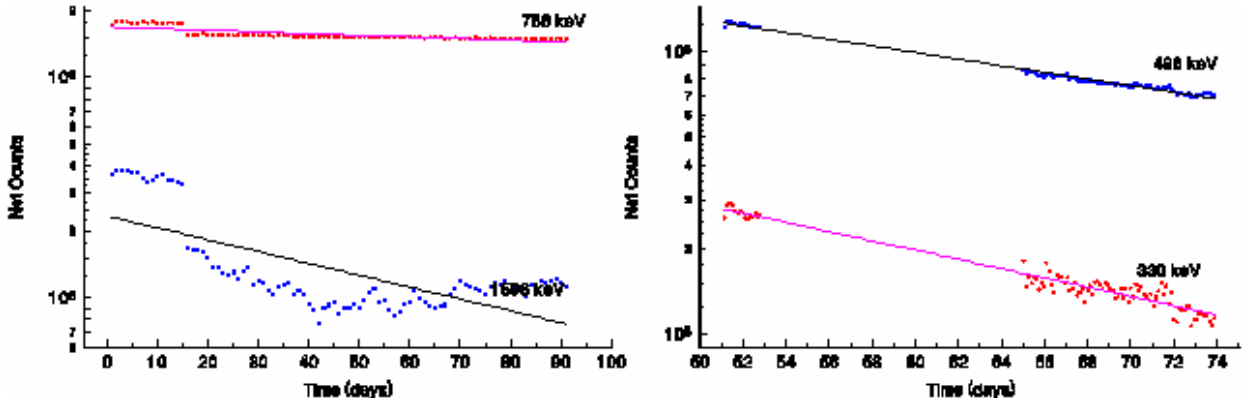

Figure 2.14: Net counts for four peaks in the NaI spectra recorded 50-75 days after irradiation

Energy (keV)	Parameters				Half lives	Composition
	A_1	λ_1 (d^{-1})	A_2	λ_2 (d^{-1})		
330	1870000	0.0375	-	-	(18.5±0.4)d	^{140}Ba (12.74d)
498	4950000	0.0268	-	-	(25.9±0.3)d	^{130}Ru (39.35d), ^{140}La Ba (12.74d)
756	2680000	0.00819	-	-	(84.6±1.3)d	^{95}Zr Nb (63.98d)
1596	8400000	0.062	-	-	(11.2±0.5)d	^{140}La (12.74d)

Table 2.23: Parameters of fits to the decay curves for four peaks in the NaI spectra recorded 50-75 days after irradiation, with corresponding half lives and compositions from table 2.14.

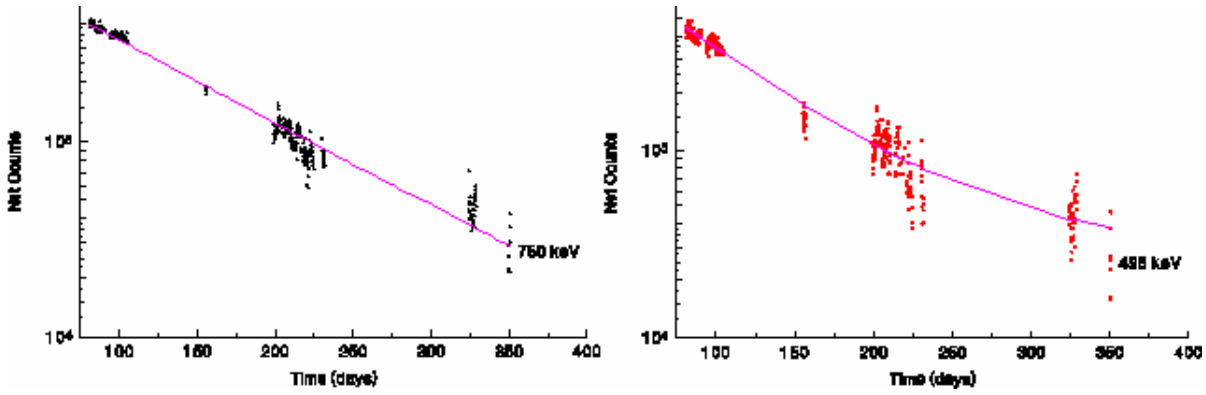

Figure 2.15: Net counts for two peaks in NaI spectra recorded 3-11 months after irradiation.

Energy (keV)	Parameters				Half lives	Composition
	A_1	λ_1 (d^{-1})	A_2	λ_2 (d^{-1})		
498	1270000	0.0140	28000	-	(49.5±1.8)d	^{103}Ru (39.35d)
750	860000	0.00969	-	-	(71.5±0.6)d	^{95}Zr Nb (63.98d)

Table 2.23: Parameters of fits to the decay curves for two peaks in the NaI spectra recorded 3-11 months after irradiation, with corresponding half lives and compositions from table 2.16.

2.8 Source Composition

During the course of the experiment γ-rays from 42 different isotopes were identified. Table 2.24 lists these isotopes in the order in which they cease to be observable in the Ge spectra, with their half lives, periods during which they were observable and additional comments mostly relating to the NaI detector. Except for ^{151}Pm and ^{137}Cs γ-rays from all these isotopes were observed in at least one detector during the first day. All the isotopes listed in table 1.1 were observed, in addition some further isotopes with half lives less than one hour were observed in the first day after irradiation.

Nuclide	Half life	Period observable	Comments
^{133}Te	12.50m	first day only	Not observed in NaI spectra
^{141}Ba	18.27m	first day only	Not observed in NaI spectra
^{131}Sb	23.00m	first day only	Not observed in NaI spectra
^{131}Te	25.00m	first day only	Not observed in NaI spectra
^{138}Cs	32.20m	first day only	Component of 2 NaI peaks
^{134}Te	41.83m	first day only	Component of two NaI peaks
^{134}I	52.60m	first day only	The major component of one NaI peak, contributes to 5 other peaks
^{133m}Te	55.40m	first day only	Minor contribution to NaI spectra
^{87}Kr	1.27h	first day only	Slight contribution to NaI spectra
^{139}Ba	1.38h	first day only	Not observed in NaI spectra
^{142}La	1.52h	first day only	Component of 2 NaI peaks
^{149}Nd	1.73h	first day only	Not observed in NaI spectra
^{88}Kr	2.84h	first day only	Major component of two NaI peaks
^{88}Rb	(2.84h)	→ 1 day	Contribution to one peak in NaI spectra
^{105}Ru	4.44h	→ 1 day	Not resolved in Ge spectra in first few hours, not observed in NaI spectra
^{135}I	6.61h	→ 2 days	Major component of 2 peaks in NaI spectra, especially from the end of day one
^{135}Xe	9.09h	→ 2 days	Major component of one NaI peak
^{91}Sr-^{91m}Y	9.52h	→ 2 days	Major component of one peak in NaI spectra at 1 day
^{93}Y	10.10h	→ 2 days	Not observed in NaI spectra
^{133}I	20.80h	→ 2 days	Major component of one peak in NaI spectra, especially at 2 days
^{105}Rh	1.47d	→ 2 days	Not observed in NaI spectra
^{97}Zr-Nb, ^{97m}Nb	16.90h	→ 1 week	Major components of NaI spectra at 1-2 days, not observed in NaI spectra at 1 week
^{151}Pm	1.18d	1 → 14 days	Not observed in NaI spectra

^{143}Ce	1.38d	1 month	Mixed with ^{99m}Tc in NaI spectra from 2 weeks
^{132}Te-I	3.26d	1 month	Major component to peaks in NaI at 2 days, clearly resolved at 1 week
^{133}Xe	5.25d	1 month	Not resolved from ^{144}Ce in LoAx
^{99}Mo-^{99m}Tc	2.75d	2 months	Major component of NaI spectra from 2 days
^{131}I	8.04d	3 months	Part of poorly resolved NaI peak from 1 day, resolved from 1 week
^{147}Nd	10.98d	6 months	Component of low energy NaI peak
^{140}Ba-La	12.74d	6 months	1596 keV peak resolved in NaI by 1 week
^{141}Ce	32.50d	entire year	Major component in NaI spectra from 2 weeks, mixed only with ^{140}Ba from 2 months
^{103}Ru	39.35d	entire year	In NaI; mixed with ^{140}Ba,La after 1 month, fully resolved after 6 months
^{95}Zr-Nb	63.98d	entire year	In NaI; mixed with ^{140}La at 1 month, resolved at six months, mixing with ^{137}Cs by 11 months
^{144}Ce	284.90d	entire year	Not resolved from ^{133}Xe in LoAx, component of low energy NaI peak from one month
^{137}Cs	30.00y	1 month	Not fully resolved from ^{95}Zr-Nb in NaI

Table 2.24: Isotopes observed in the experiment, with their half lives and the periods over which they were observed. The comments relate mostly to the NaI detector. The isotopes are listed in the order in which they cease to be observable in the Ge spectra.

3. SOURCE TERM AND γ-RAY SPECTRUM SIMULATION

3.1 Nuclear Fission

Nuclear fission is the process whereby heavy nuclei, typically actinides, split into two lighter nuclei, with an accompanying release of energy. For several nuclei fission follows the capture of a thermal neutron; such nuclei are said to be fissile. Nuclear reactors operate on a chain reaction in which a fissile nucleus (usually ^{235}U) absorbs a thermal neutron (ie neutrons which are in thermal equilibrium with the reactor, with energies of about 0.03eV) which induces fission. The fission releases energy and a number of fast neutrons, these neutrons are then moderated, slowing them down to thermal energies. If, on average, one of these neutrons is absorbed by another fissile nucleus resulting in fission then a self-sustaining chain reaction occurs, and the reactor is said to be critical. If, on average, more than one neutron is absorbed by a fissile nucleus then the reactor is said to be super-critical, if less than one neutron is absorbed the reactor is sub-critical.

Following fission a broad range of products is formed with masses mostly in the range from 60-170 atomic mass units (amu's); the yield of any one isotope being at most a few percent. Most of the nuclei formed are unstable, having an excess of neutrons, and decay by β-emission (with half lives ranging from milliseconds to several years), or very occasionally by neutron emission (with half-lives of less than a few seconds).

The radioisotope inventory of a nuclear reactor consists of a complex cocktail of fuel material, fission products, decay products and activation products caused by the capture of neutrons by other material in the reactor (fuel cladding, moderators, structural materials etc.). The composition of this inventory will change over time as fission products are produced, and then decay or absorb neutrons. In the event of an accident the composition of the radionuclides released will depend upon the current radioisotope inventory of the reactor and the type and severity of the accident.

The fission rate in a reactor (R_f) depends on the number of fissile nuclei present (N_U), the neutron flux (φ) and the fission cross section (σ_f).

$$R_f = N_U \varphi \sigma_f \tag{3.1}$$

The number of any particular isotope formed by fission (dN_f) during a time interval (dt) will depend on the fission yield (Y_f) for that isotope.

$$dN_f = R_f Y_f dt \tag{3.2}$$

The isotopes thus formed then decay, usually by β-decay, with a characteristic half-life ($t_{½}$). The number that decay (dN_d) depends on the number present (N) and a decay constant (λ). The number of daughter isotopes also increases by the same amount. Where there is more than one decay path the increase in population is divided between the daughter isotopes according to a branching ratio.

$$dN_d = N\, e^{-\lambda dt} \tag{3.3}$$

The population of a particular isotope will also decrease as a result of neutron capture (or "burn-up"), depending on the neutron capture cross section (σ_c). There will also be a corresponding increase in the population of the resulting isotope.

$$dN_c = N \varphi \sigma_c dt \tag{3.4}$$

The resulting change in the population of a particular isotope in time interval dt is thus the product of these processes.

$$dN = dN_f - dN_d - dN_c + dN_d' + dN_c' \tag{3.5}$$

Where dN_d' and dN_c' are the changes in population due to the decay of and neutron capture by other isotopes. To simulate a fission product inventory one simply has to evaluate dN for all isotopes formed in the fission process or by neutron capture by fission products over a series of time intervals.

3.2 Simulation Code Development

A simple code to simulate fission product inventories has been developed using the C++ programming language (Cresswell 1997). It assumes that fission of ^{235}U induced by thermal neutrons is the only fission process that occurs, ie: it ignores fission induced by fast neutrons on ^{235}U or fission of other isotopes. The formation of activation products by neutron capture on reactor material is also ignored, as is the production of trans-uranic isotopes by neutron capture on fuel. The code also assumes that the neutron flux is constant throughout the entire mass of fissile material and fission products.

The code consists of a series of modules which handle the nuclear data and the population of the isotopes of interest, the simulation of fission product inventories, the simulation of the decay of inventories and various file handling functions. The relationship between these modules is shown in figure 3.1, and details of each module are given below.

The Nuclear Data and Population Module

The nuclear data and the population of nuclear states is handled by a class (which is a C++ data structure containing mixed data types and functions). For each isotope and metastate nuclear data for independent and cumulative fission yields, half-lives, thermal neutron capture cross-sections, decay modes and γ-ray energies and intensities are stored. In addition, there are variables for the population and change in population of each state. The data used was derived from the JEF 2.2 database using the JEF-PC package (OECD 1994).

The class also contains a number of functions to allow other parts of the program to access the data, and to read or write to the population information. Upon execution the class is initialised, at which point the nuclear data is loaded from an ASCII file. This provides flexibility in the data used by the simulation, allowing the inclusion of further data (eg: data for reactor materials and their activation products). At present the program uses data for 785 nuclear states.

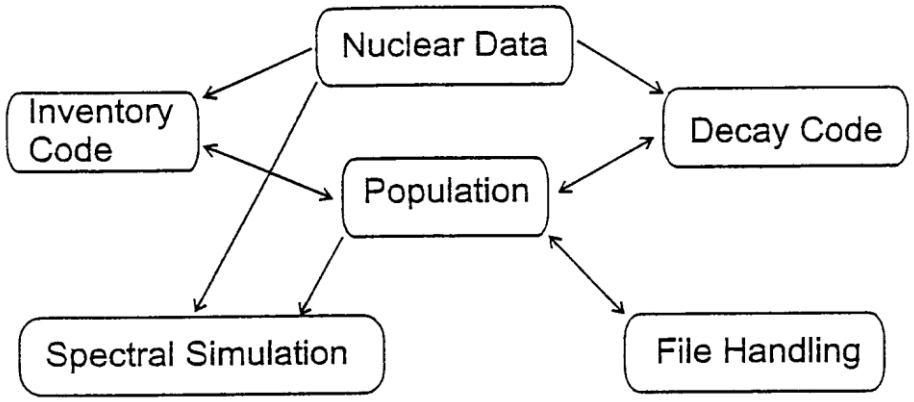

Figure 3.1: The relationship between the different modules of the simulation code.

The Simulation Code Module

The program loops through all the nuclear states calculating the change in population for each using equation 3.5, for an initial mass of ^{235}U, neutron flux and time interval entered by the user. After each loop the population of each state is updated, and the simulation time increased by the time interval until the final simulation time (which is also entered by the user) is reached. This routine is illustrated in figure 3.2.

The Decay Code Module

The decay code module is the similar to the simulation code module, except that only the decay terms are considered. The user inputs the simulation time and time interval, the ^{235}U mass and neutron flux are not required.

The Spectral Simulation Module

The spectral simulation module uses the population information and the γ-ray energies and intensities from nuclear data to produce simulated γ-ray spectra. The code calculates the activity of each isotope, and then the associated γ-ray information is collated into a line spectrum at 1 keV per channel. This spectrum is then compressed into a 5 keV per channel array from which a simulated NaI spectrum is formed by using spectra produced by separate Monte Carlo codes. These are calculated for a source on a concrete surface with the detector either 1.6m or 50m above it for γ-ray energies at 5keV intervals. These spectra are stored as ASCII files and recalled when needed. The total spectrum is formed by summing the spectra corresponding to each of the channels in the compressed array multiplied by the intensity of that channel. Spectra were simulated for channels with intensities greater than 1% of the maximum intensity, for channels with less intensity a nearby spectrum (within 50KeV) was used and stretched to the correct energy using the technique of Paatero 1964. Two Monte Carlo codes had been developed previously to simulate the response of AGS detectors to natural radiation fields and some generalized

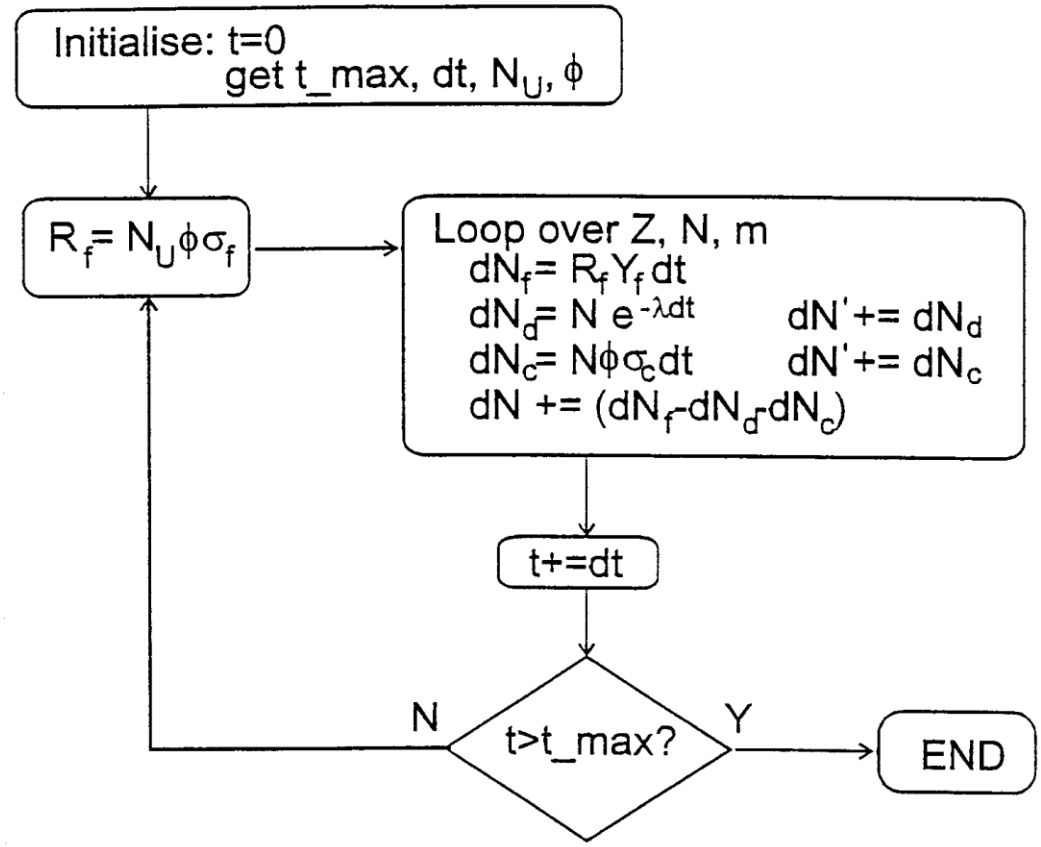

Figure 3.2: Schematic of the inventory simulation module. The decay module is similar, except only the decay term dN_d is used.

anthropogenic sources (Allyson 1994, Allyson & Sanderson 1997). A full analogue code (MCI) was validated and experimentally used for the close-coupled geometries. For AGS geometries a statistical estimation technique (MCII) was developed to increase simulation speeds. For this work a further code incorporating an inverted source-detector geometry was developed (MCIII), which results in further efficiency improvements for uniform planar sources (Allyson 1997).

In addition to producing the NaI spectrum it is also possible to output the 1keV per channel line spectrum. It is also possible to produce NaI spectra for a single mass chain or isotope in addition to the entire inventory. This information, along with the activities of all the states in the source, enables one to quantify the contributions of each state to the peaks in the NaI spectra, and produce spectra for each of these components. This is a potentially very useful tool in spectral deconvolution studies, although it has not been used for this purpose in the current study.

The File Handling Module

The file handling module handles the saving and loading of the inventory data. The data are saved as ASCII files consisting of a user supplied header string identifying the file contents, the number of ^{235}U nuclei and the fission product inventory saved as a string identifying the isotope (as "A[m]X", where A is the mass, 'm' is included for metastates, and X is the elemental symbol), the number of nuclei and activity in becquerels, and a file terminator. The file format allows one

to enter inventories from other sources (eg: the source terms of past accidents). Data can be saved either from the main menu, at the end of a simulation or automatically at intervals during a simulation. In the later instance the time into the simulation is added to the header string. When loading the inventory data the option of replacing or adding to existing data is given. An additional routine allows the output of the fractional contribution of the activity of each state to the total source activity. This can be given in isotopic order or in order of decreasing activity, and an activity threshold can be used.

3.3 Verification of Code

In order to verify that the simulation code was working correctly, it was run to produce simulated spectra for the previously measured experimental system. The spectra were normalized to the experimental spectra using the known livetimes, and geometrical correction factors determined from spectra recorded with the calibration sources. Figure 3.3 shows six of these simulated spectra with the corresponding experimental spectra.

It can be seen that, with a few exceptions, there is good agreement between the simulated and measured spectra. The exceptions are peaks in the experimental spectra due to poorly subtracted background, particularly from the 2614keV ^{208}Tl peak, and the high low energy background at 3 hours (spectrum (a)) due to scatter from the sides of the floor pit. One significant difference between the experimentally measured and simulated spectra is the absence of the shoulder on the 750keV peak at 6 months (spectrum (f)) due to ^{137}Cs. The contribution of ^{137}Cs calculated from the Ge spectra and the simulation both agree, and are both insufficient to account for the experimentally observed shoulder. The shoulder is probably due to incomplete subtraction of a laboratory background.

The simulation output includes the activities of each fission fragment and a list of γ-ray energies (to 1keV) and intensities. From these it is possible to determine the main components of each of the peaks in the NaI spectra, which can be used to confirm the identifications derived from the Ge spectra. Table 3.1 compares the identification of selected peaks determined from the simulation and experimental measurements. It can be seen that, for most peaks, the agreement is very good, confirming that the simulation code accurately models the experimental data.

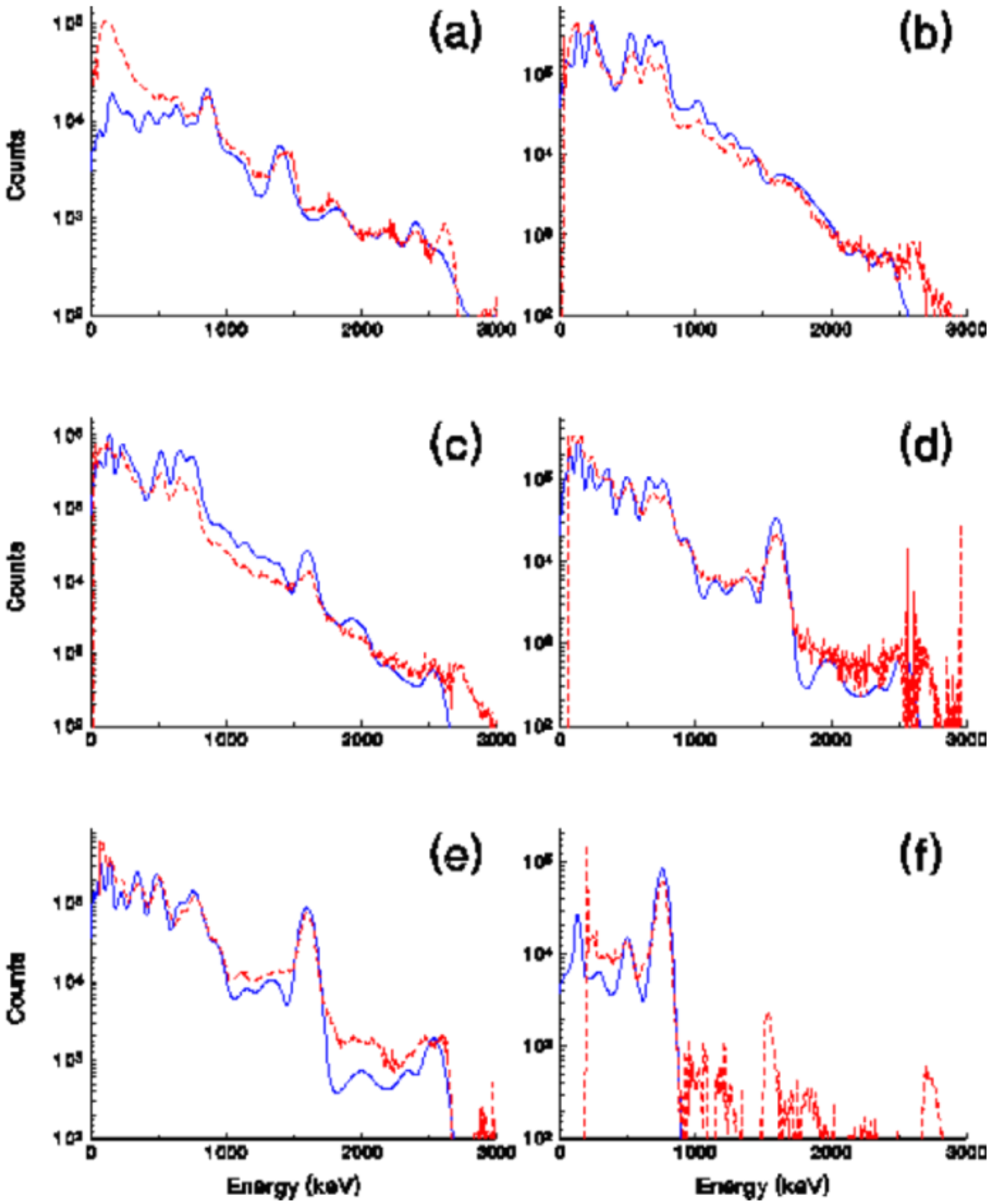

Figure 3.3: Spectra generated by the simulation of the experimental system (solid lines) with the corresponding experimentally measured spectra (dashed lines) for six different periods after irradiation. (a) 3 hours, (b) 1 day, (c) 2 days, (d) 7 days, (e) 14 days and (f) 6 months after irradiation.

Peak Energy (keV)	Time after irradiation	Main isotopic contributions	
		Experimental	Simulation
114	2 days	^{99m}Tc ^{99}Mo 70%, ^{133}Xe 20%	^{99m}Tc ^{99}Mo 70%, ^{131}Te 20%
144	7 days	^{99m}Tc ^{99}Mo 70%, ^{141}Ce 20%	^{99m}Tc ^{99}Mo 75%, ^{141}Ce 15%
222	1 day	^{135}Xe 75%, ^{132}Te 20%	^{135}Xe 50%, ^{132}Te 20%, ^{143}Ce 20%
366	7 days	^{131}I 90%, ^{143}Ce 7%	^{131}I 65%, ^{140}La 17%, ^{143}Ce 12%
505	7 days	^{140}Ba-La 50%, ^{132}I 20%, ^{103}Ru 15%	^{140}Ba-La 60%, ^{103}Ru 15%, ^{132}I 12%
510	2 days	^{133}I 50%, ^{132}I 10%, ^{140}La 10%, ^{91m}Y 10%	^{133}I 60%, ^{140}Ba-La 10%, ^{91m}Y 10%
516	1 day	^{133}I 60%, ^{91m}Y 25%, ^{97}Zr 5%	^{133}I 65%, ^{91m}Y 25%
528	3 hours	^{133}I 30%, ^{91m}Y 25%, ^{134}I 20%	^{91m}Y 30%, ^{133}I 30%, ^{134}I 20%
654	2 days	^{132}I 45%, ^{97}Nb 45%	^{97}Nb ^{97}Zr 50%, ^{132}I 45%
642	3 hours	^{142}La 40%, ^{134}I 30%, ^{97}Nb 15%	^{142}La 40%, ^{134}I 25%, ^{97}Nb 20%
666	7 days	^{132}I 95%	^{132}I 85%, ^{131}I 5%
648	1 day	^{97}Nb 65%, ^{132}I 20%, ^{91}Sr 5%	^{97}Nb 85%
744	2 days	^{97m}Nb 45%, ^{132}I 35%, ^{143}Ce 5%	^{97m}Nb 45%, ^{132}I 30%
744	1 day	^{97m}Nb 55%, ^{132}I 15%, ^{91}Sr 10%	^{97m}Nb 55%, ^{132}I 15%, ^{91}Sr 10%
750	6 months	^{95}Zr-Nb 98%, ^{137}Cs 2%	^{95}Zr-Nb 98%, ^{137}Cs 1%
774	7 days	^{132}I 45%, ^{95}Zr 20%, ^{140}La 15%, ^{99}Mo 10%	^{132}I 55%, ^{95}Zr 25%, ^{99}Mo 10%
864	3 hours	^{134}I 80%, ^{133m}Te 10%	^{134}I 85%, ^{133m}Te 7%
942	7 days	^{132}I 60%, ^{140}La 30%	^{132}I 45%, ^{140}La 40%
1014	1 day	^{91}Sr 85%, ^{135}I 13%	^{91}Sr 75%
1116	1 day	^{135}I 60%, ^{131m}Te 20%, ^{97}Zr 10%	^{135}I 50%, ^{131m}Te 15%, ^{97}Zr 15%
1266	1 day	^{135}I 70%, ^{133}I 25%	^{135}I 55%, ^{132}I 15%
1380	3 hours	^{92}Sr 75%, ^{138}Cs 25%	^{92}Sr 65%, ^{138}Cs 25%
1392	7 days	^{132}I	^{132}I 95%
1446	1 day	^{135}I 70%, ^{91}Sr 15%	^{92}Sr ^{92}Y 45%, ^{135}I 25%, ^{132}I 20%
1590	2 days	^{140}La 95%, ^{135}I 5%	^{140}La 98%
1596	7 days	^{140}La	^{140}La 99%
1830	3 hours	^{88}Rb 45%, ^{134}I 30%, ^{135}I 20%	^{88}Rb 35%, ^{134}I 25%, ^{142}La 20%
2400	3 hours	^{88}Kr 55%, ^{142}La 45%	^{88}Kr 55%, ^{142}La 40%

Table 3.1: Comparison between compositions of selected NaI peaks determined experimentally from Ge spectra and from the simulation.

3.4 Simulation of airborne geometry

Spectra corresponding to an airborne geometry, with the detector place 50m above a uniform plane deposition with the same isotopic composition as the simulated experimental sources, were also simulated. Figure 3.4 shows some of the resulting spectra with the corresponding close-coupled simulated spectra for comparison. The airborne spectra shown in this figure have been scaled by arbitrary factors to produce spectral features of similar intensities to the close-coupled geometry spectra, and thus ease comparison between the two. The airborne spectra are similar to the ground based spectra, except at energies below about 600keV where the scattering of γ-rays by the intervening atmosphere creates a large background which swamps the peaks in this region. However, this background can be removed from experimental spectra by the use of altitude dependent stripping factors, which can be determined from experimental measurements or Monte Carlo simulation (Allyson 1994, Allyson & Sanderson 1997).

3.5 Simulation of long irradiation periods

The spectra described so far, both experimental and simulated, have been produced by sources that have undergone short irradiation periods of at most 1.5 hours. However it would be expected that the source term from real nuclear accidents would be from material that had experienced much longer irradiation periods. The code has been used to simulate a six month irradiation of ^{235}U, with full retention of fission products, to provide further information on the spectra that would be observed from more realistic source terms. Simulated airborne NaI spectra for various times after irradiation were produced, some of which are shown in figure 3.5 with the corresponding spectra for a short irradiation for comparison. The major components of the peaks in these spectra are given in table 3.2.

These spectra clearly show the greater influence of longer lived isotopes, with a corresponding reduction in the contribution of shorter lived isotopes. This is particularly noticeable in the earlier spectra where the ^{140}La peak at 1596keV is present in the spectra produced following the longer irradiation but not in the spectra for the short irradiation. Conversely, the 864keV peak due to ^{134}I is present in the 3 hour spectrum for a short irradiation, but absent in the spectrum for longer irradiation times. For later periods after irradiation the spectra for short and long irradiations become progressively more alike.

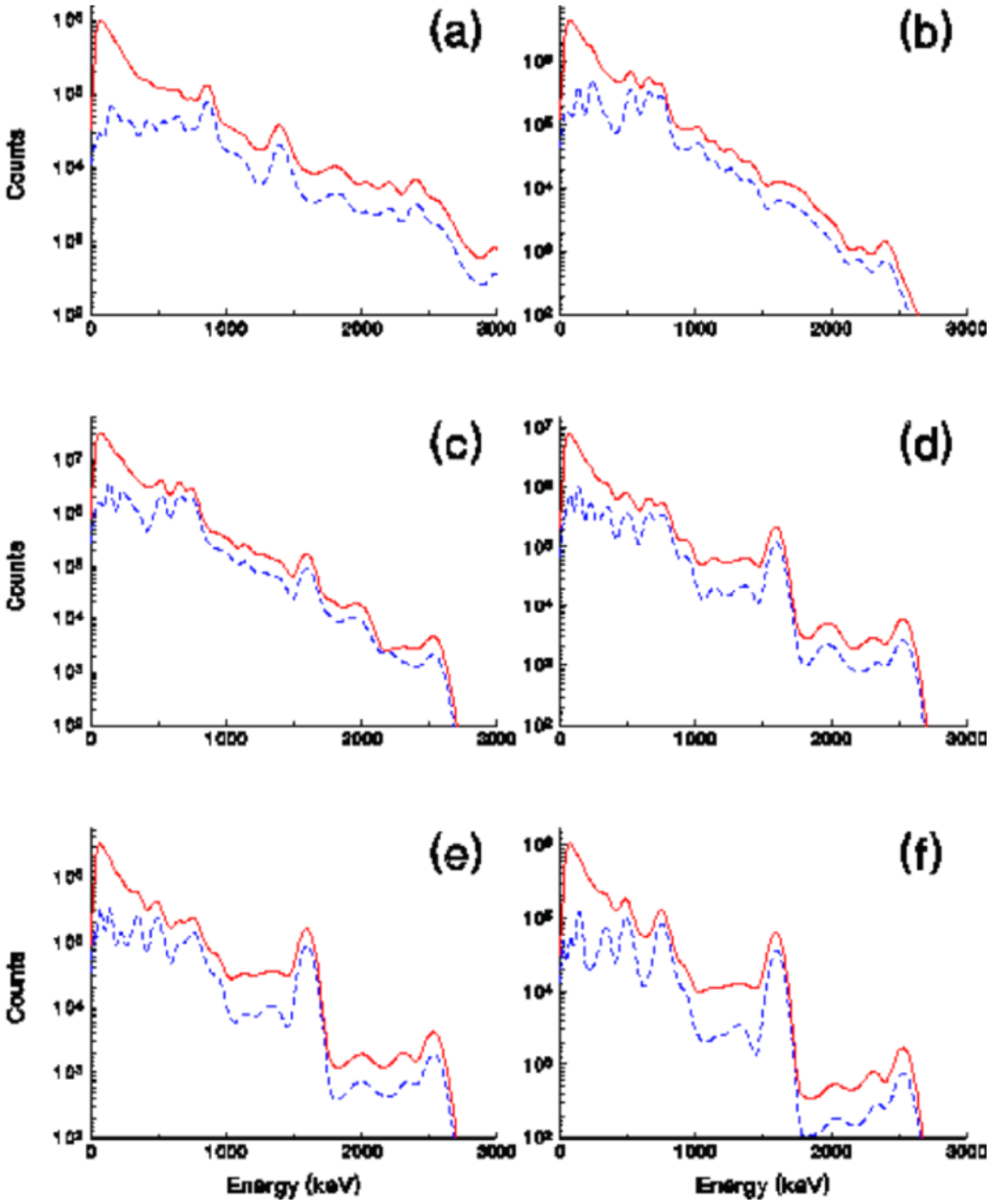

Figure 3.4: Spectra generated by the simulation of the experimental sources for airborne geometry (solid lines) with the corresponding ground based simulated spectra (dashed lines) for six different periods after irradiation. (a) 3 hours, (b) 1 day, (c) 2 days, (d) 7 days, (e) 14 days and (f) 1 month after irradiation.

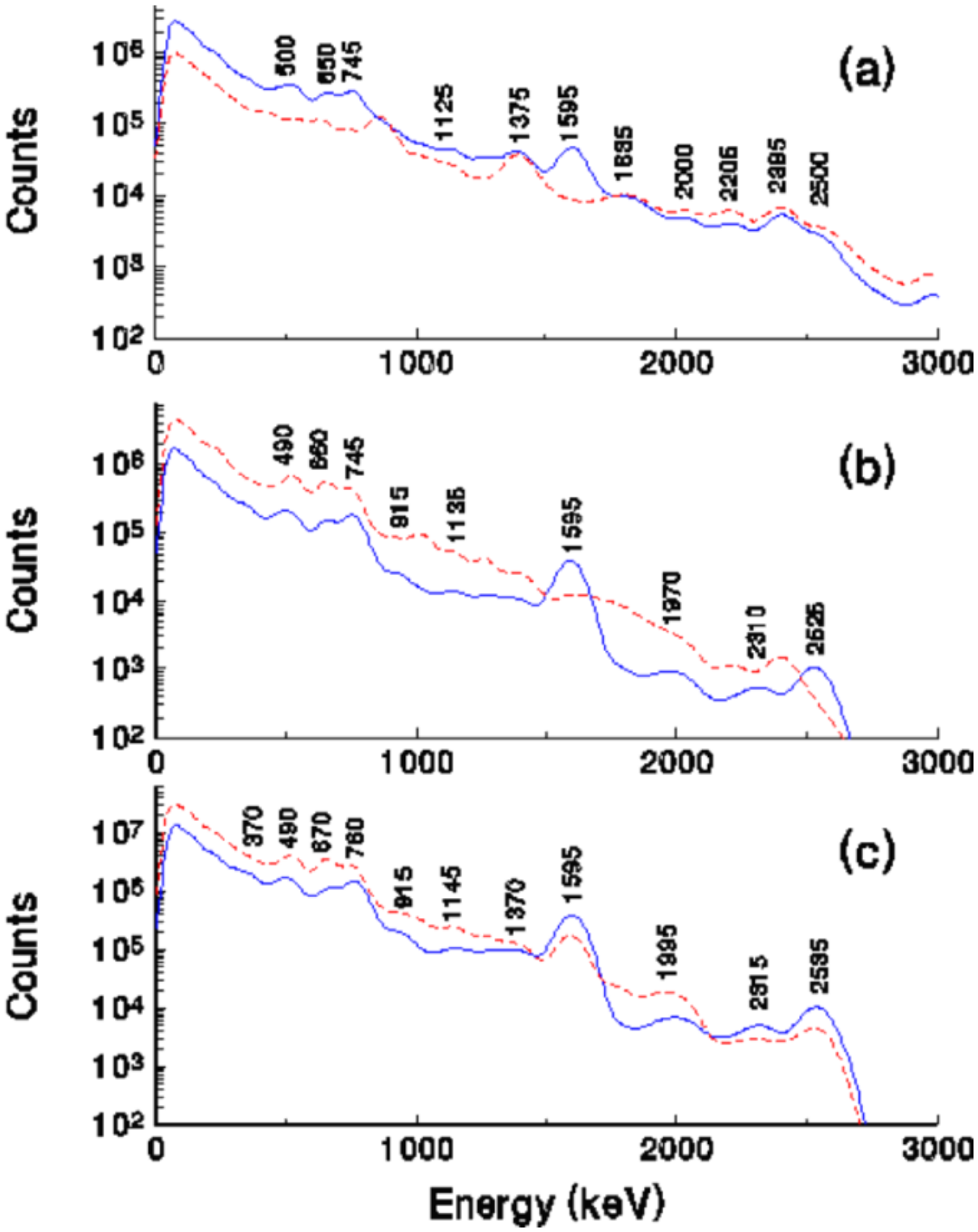

Figure 3.5: NaI spectra, for the airborne geometry, for sources produced by long (solid lines) and short irradiation (dashed lines) periods, at (a) 3 hours, (b) 1 day, and (c) 2 days after irradiation. With the energies of peaks in the spectrum produced from the long irradiated source indicated.

Peak Energy (keV)	Time	Composition
370	2 days	^{143}Ce 30%, ^{131m}Te 25%, ^{99}Mo 15%
490	1 day	^{133}I 55%, ^{140}Ba 25%
490	2 days	^{140}Ba 35%, ^{133}I 30%, ^{132}I 15%
500	3 hours	^{140}Ba 40%, ^{132}I 25%, ^{135}Xe 13%, ^{147}Nd 8%, ^{97}Zr 7%
650	3 hours	^{132}I 45%, ^{97}Nb 40%
660	1 day	^{132}I 80%
670	2 days	^{131}I 70%, ^{97}Nb 15%
745	3 hours	^{95}Zr-Nb 70%, ^{132}I 20%
745	1 day	^{95}Zr-Nb 55%, ^{132}I 12%, ^{97m}Nb 10%
760	2 days	^{132}I 30%, ^{95}Zr 30%, ^{140}La 20%, ^{97m}Nb 10%, ^{99}Mo 10%
915	1 day	^{140}La 65%
915	2 days	^{140}La 90%
1125	3 hours	^{135}I 50%, ^{131m}Te 10%, ^{134}I 8%
1135	1 day	^{131m}Te 35%, ^{135}I 30%, ^{132}I 28%
1145	2 days	^{132}I 50%, ^{131m}Te 25%
1370	2 days	^{132}I 80%, ^{133}I 10%
1375	3 hours	^{92}Sr 60%, ^{132}I 20%
1595	3 hours-2 days	^{140}La
1835	3 hours	^{88}Rb
1970	1 day	^{132}I 55%, ^{131m}Te 25%, ^{93}Y 10%
1995	2 days	^{132}I 75%, ^{131m}Te 15%
2000	3 hours	^{88}Kr 45%, ^{132}I 30%, ^{135}I 20%
2205	3 hours	^{88}Kr 70%, ^{142}La 10%
2310	1 day	^{140}La 75%
2315	2 days	^{140}La
2395	3 hours	^{88}Kr 55%, ^{142}La 10%
2500	3 hours	^{140}La 75%, ^{142}La 15%
2525	1 day	^{140}La
2535	2 days	^{140}La

Table 3.2: Composition of peaks in the simulated NaI spectra for a long irradiation period.

4. DISCUSSION

Over the course of a year gamma-ray spectra were recorded from a fission product source using three different detectors and two spectrometry systems. Analysis of these spectra showed that most of the peaks arise from an initial set of 42 different isotopes which could be resolved using the Ge detectors. This set of isotopes simplified rapidly; after one day some 28 isotopes remained, by one week this had reduced to some 20 isotopes, by one month to 18, and by 6 months to 7 isotopes. The NaI detectors were able to resolve some of these nuclides at all stages, albeit with interferences which would need to be stripped out, particularly at the early stages.

Those isotopes most readily measurable in the experimental NaI spectra are listed in table 4.1 with the period over which they were observed and the peaks which they contributed to. Inert gases have not been included in this table. In the event of an accidental release of fission products these would not be expected to contribute to deposited activity, which we take to be the principle target for airborne gamma spectrometry. However, noble gases could contribute to spectra recorded from any plume, and may well represent a significant external dose contributor. From this point of view the most significant isotopes would be ^{87}Kr, ^{88}Kr and ^{135}Xe, all of which would be detected over the first few days. From table 4.1 it is possible to indicate how one might undertake the mapping of radiologically important nuclides deposited after an accident using NaI spectrometers. While such high volume scintillation detectors are not able to resolve the full range of nuclides, they are clearly able to retrieve information on important sets of nuclides.

Dealing with the earliest stages first, it is notable, and possibly not widely recognised, that ^{92}Sr ($t_{½}$ = 2.71 h) and ^{91}Sr ($t_{½}$ = 9.52 h) both have high fission yields with sufficiently high energy γ-ray emission to be readily detected within the first day or two using AGS systems. The significance of this is observation is that ^{89}Sr and ^{90}Sr are pure β-emitters which are difficult to quantify in the environment, but can potentially contaminate milk and accumulate in bone. In past accidents considerably less is known about the spatial distribution of Sr isotopes than the more readily determined I or Cs isotopes, partly as a consequence of the need for radiochemical separations in their determination. The possibility of inferring the distribution of β-emitting Sr isotopes by γ-ray surveys represents a potentially important role for AGS, and one which has not previously been recognised. However to be effective it would depend on (i) the release of activity taking place within 1-2 days of irradiation and (ii) rapid deployment of the survey, since the window of opportunity for detection of ^{92}Sr and ^{91}Sr is short. It should be borne in mind that rapid deployment may raise the risks of contaminating the aircraft, and that these should be balanced against the value of the information which could be gathered.

The iodine isotopes are another critically important group of radiologically important nuclides, since they are volatile, and thus likely to be released in an accident. Furthermore, if inhaled or ingested, they can accumulate in the thyroid with a resulting increased chance of thyroid cancer. In the NaI spectra, ^{134}I ($t_{½}$ = 52.6 m) and ^{133m}Te ($t_{½}$ = 55.4 m) produce a single peak at 864keV that is resolved for the first five hours after irradiation. After a few hours the ^{135}I ($t_{½}$ = 6.6 h) peak at 1458keV and the ^{133}I ($t_{½}$ = 20.8h) peak at 530keV are readily quantifiable for a couple of days. The longer lived isotopes ^{132}I (with its associated ^{132}Te parent, $t_{½}$ = 3.26d) and ^{131}I ($t_{½}$ = 8.04 d) are quantifiable after one day and one week respectively, although both require the stripping out of other components. Both of these isotopes remain quantifiable for several weeks. It is evident

Isotope	Half life	Period quantifiable	Method of measurement
^{134}I ^{133m}Te	52.60m 55.40m	→ 5 hours	864keV peak composed of 864keV ^{1334}Te and 847keV, 884keV ^{134}I γ-rays.
^{142}La	1.52h	→ 10 hours	2400keV peak composed of 2398keV and 2543keV ^{142}La and 2392keV ^{88}Kr γ-rays
^{92}Sr	2.71h	→ 15 hours	1380keV peak due largely to 1384keV ^{92}Sr γ-rays
^{135}I	6.61h	5 hours → 2 days	1494keV peak composed of 1458keV ^{135}I and 1530keV ^{88}Kr γ-rays
^{133}I	20.80h	5 hours → 3 days	522keV peak has strong 530keV ^{133}I γ-rays component
^{97}Zr-Nb	16.90h	10 hours → 5 days	648keV peak composed of 658keV ^{97}Nb and 621keV, 630keV ^{132}I γ-rays 744keV peak composed of 743keV ^{97m}Nb and 772keV ^{132}I γ-rays
^{91}Sr	9.52h	1 day → 2 days	1014keV peak composed of 973keV, 1039keV ^{135}I and 1024keV ^{91}Sr γ-rays
^{132}Te-I	3.26d	1 day → 2-3 weeks	222keV peak composed of 228kev ^{132}Te and 250keV ^{135}Xe γ-rays 942keV peak composed of 952keV ^{132}I and 925keV ^{140}La γ-rays (subtracting ^{140}La from 2 days) 1392keV peak composed of 1372keV and 1399keV ^{132}I γ-rays from 5 days
^{99}Mo ^{99m}Tc	2.75d	2 days → 2 months	144keV peak composed of 141keV ^{99m}Tc and 81keV ^{133}Xe γ-rays, with 145keV ^{141}Ce γ-rays from 7 days. If threshold is not too high
^{140}Ba-La	12.74d	2 days → 6 months	1596keV peak due to 1596keV ^{140}La γ-rays
^{131}I	8.04d	1 week → 1 month	348keV peak composed of 284keV, 365keV ^{131}I and 305keV, 329keV ^{140}Ba-La γ-rays (subtracting ^{140}Ba-La)
^{95}Zr-Nb	63.98d	from 1 week	750keV peak composed of 724keV, 757keV, 766keV ^{95}Zr-Nb and 752keV ^{140}La γ-rays (subtracting ^{140}La) also 661keV ^{137}Cs γ-rays from 10 months
^{103}Ru	39.35d	from 1 week	498keV peak composed of 497keV ^{103}Ru and 424keV, 487keV ^{140}Ba-La γ-rays (subtracting ^{140}Ba-La)
^{137}Cs	30.00y	from 6 months	Shoulder on side of 750keV peak due to 661keV γ-ray

Table 4.1: The isotopes that are readily quantifiable in the NaI spectra recorded in this experiment at various stages after irradiation, giving the approximate periods when they are identifiable, with details of the peaks they are measurable in and what, if anything, would need stripping out.

from the data examined in this project that the preferred I peaks and interferences which would need to be stripped out change rapidly over the first few days after irradiation. Nevertheless it would be possible to quantify I nuclides (using an appropriate time dependent model) at all stages. The volatility of these nuclides has been noted, and it is further notable that after both the Windscale fire in 1957 and the Chernobyl accident, where I nuclides comprised a major component of the environmental source terms, that ^{131}I was detected by AGS methods (Williams et. al. 1958, Mellander 1989, Grasty et. al. 1997).

Table 4.1 also shows that a range of less volatile and non-volatile fission products are also detectable. Of these ^{99}Mo-^{99m}Tc ($t_{½}$ = 2.75d) could be detected in the low energy spectral region (<150 keV) providing the aircraft altitude was low, and the spectrometer mounted and operated in an appropriate manner. Stripping the general scattered contribution to these energy regions would be necessary. The non-volatile Zr-Nb (^{97}Zr, $t_{½}$ = 16.9 h and ^{95}Zr, $t_{½}$ = 63.98 d) and Ba-La (^{142}La, $t_{½}$ = 1.52 h and ^{140}Ba, $t_{½}$ = 12.74 d) isotopes also produce prominent signals in NaI detectors. The extent to which these would be present in accident conditions clearly depends on the release scenario. Past experience (Sanderson et. al. 1997) offers two distinct cases. The reactor accidents at Windscale and Chernobyl clearly resulted in preferential release of more volatile components, reflected in the γ-ray spectra measured, particularly at great distances from the accident. The spectra recorded after the Cosmos-954 re-entry in Northern Canada (Bristow 1978, Grasty 1980) however show preferential remains of non-volatile components, which survived atmospheric burn-off. Our experimental results from unseparated sources confirm that both ^{95}Zr and ^{140}La were readily detected over substantial periods.

Another important isotope is ^{137}Cs, which in our experiment produces a shoulder on the side of the larger 750keV ^{95}Zr-Nb peak after 6 months in the NaI spectra, but is resolved in the Ge spectra after 1 month. The relative lack of ^{137}Cs in these data is probably a result of the short irradiation time used for these samples, which significantly enhanced the contribution of shorter lived isotopes to the spectra. The simulated spectra do not produce the shoulder on the 750keV peak, even for a longer irradiation period. The shoulder observed in the experimental spectra may be due to laboratory background. The simulation predicts very low ^{137}Cs levels, with the γ-activity only 1% that of ^{95}Zr-Nb after 6 months for the short irradiation, and 4% for the long irradiation. Even for the six month simulated irradiation the γ-activity of ^{137}Cs would only reach 10% of ^{95}Zr-Nb activity after approximately one year. In more realistic scenarios with differentiation of fission products on release the greater volatility of Cs will significantly enhance the ^{137}Cs signal. This situation clearly applied to the Chernobyl accident, where Cs levels were also enhanced by the greater fuel age than considered here, and by the presence of ^{134}Cs, produced by activation of reactor impurities.

Overall therefore the results have shown that NaI spectrometers can potentially provide quantitative information on Sr, I, Cs and nonvolatile nuclides at different stages of response to a reactor accident. The particular energies detected, and interferences to be resolved by stripping, change rapidly in the early stages. However it is clear both from the simulations conducted, and from the experience of past accidents, that the characteristics of accident source terms tend to simplify the range of nuclides to be considered at any one stage. The practical capabilities of NaI spectrometers are thus dependent on the source term, and in particular on the extent to which volatile and non-volatile components are separated during and following release. Information on the relative proportions of such components in deposited activity would also simplify analysis of

NaI spectra.

The greater resolution of Ge detectors allows the separation of more isotopes, or their identification at earlier times after irradiation. Whether used as part of an AGS system, or deployed at ground level, these detectors are more capable of defining the isotopic composition of both deposited activity and of the source term. The detection efficiency however is considerably lower than NaI detectors, which would lead to lower count rates and longer measurement times. However count rates in areas of high deposition should be sufficient both to generate statistically significant spectral information, and for nuclide specific mapping. Ge detectors are generally less robust, and may prove less reliable under emergency conditions, but they could provide valuable data, which would complement NaI detectors, in the event of an accidental release of radioactive material.

The use of Ge detectors produces peaks due to iodine isotopes that require very little stripping to quantify. In particular, during the first day there are peaks due to ^{133}I γ-rays at 530keV, ^{134}I γ-rays at 541keV, 595keV, 622keV, 847keV, 884keV, 1073keV and 1742keV, and ^{135}I γ-rays at 1132keV, 1260keV, 1458keV, 1678keV. At later times there are also peaks due to ^{131}I γ-rays at 365keV and ^{132}I γ-rays at 431keV, 523keV, 668keV (which may interfere with ^{137}Cs γ-rays at 661keV), 910keV, 955keV, 1372keV, 1399keV and 2002keV. Using Ge detectors to quantify these peaks would allow the activity due to the different iodine isotopes to be calculated. This would allow the measurements of one isotope with a NaI detector to be used to estimate the activity of the other isotopes. It could also be used to find the time since irradiation ceased, since the activities of these isotopes would equilibrate in the reactor after ~1 month (four half lives of ^{131}I) of constant power operation.

In Ge spectra the 662keV ^{137}Cs γ-ray was not fully resolved from the ^{132}I 668keV γ-ray in the spectra recorded in this experiment, due largely to the relative weakness of the Cs signal. In an accident where a larger proportion of Cs is released the two can be resolved using laboratory based Ge detectors, but they might not be resolved in the field. However, the ^{132}I component can be stripped out using the activities of other ^{132}I γ-rays.

In addition to the experimental evidence discussed above, a computer code was developed to simulate fission product sources and NaI spectra, and has been used to confirm the experimentally derived compositions of the peaks in the NaI spectra and to investigate the dependence on source-detector geometry and irradiation history. The agreement between simulation and experimental data for the NaI system was good, the simulated data reproducing the majority of time dependent features recorded under experimental conditions. The simulation model was then used to investigate the effects of longer irradiation on expected spectra, and the effects of the introduction of an air path between source and detector equivalent to AGS conditions.

The effect of longer irradiation is to enhance longer lived components relative to the shorter lived. This is evident in the simulated spectra for a longer irradiation time, where the 864keV peak due to ^{134}I and ^{133m}Te is no longer evident and the contribution of the longer lived ^{131}I and ^{132}I isotopes is much greater. In addition, the much greater strength of the ^{140}La peak at 1596keV strongly interferes with the 1458keV ^{135}I peak, and there are significant interferences between ^{140}Ba and the 530keV ^{133}I peak. The simulation of the aircraft geometry showed an increase in scattered

radiation and decrease in full-energy peak heights, particularly at low energies, in a manner which is consistent with both expectations, and with experience of environmental surveys conducted at different heights. This simulation procedure could be extended in future to model the source terms for past accidents, or to model hypothetical source terms for potential accidents, such as the design reference accidents for current reactor types. The most complex source term for previous nuclear accidents was that from Chernobyl. Estimates of this source term include up to 30 radioisotopes including actinides and low γ-yield isotopes, the γ-ray spectra recorded after this accident included peaks from up to 22 different isotopes (Sanderson et. al. 1997). This compares with the 42 isotopes measured in the spectra recorded in this experiment. Given the importance of nuclide distribution and segregation during the accident in determining the spectra observed, and the need for stripping to extract nuclide specific information from the NaI spectra, it would be worth simulating these additional cases in the future to facilitate preparation of spectral analysis procedures appropriate to emergency response.

5. CONCLUSION

An experiment has been conducted to evaluate the response of gamma-ray spectrometry systems to fission product sources. This consisted of sealed samples of ^{235}U briefly irradiated, with the resultant γ-rays measured over the course of one year using three detector systems; a 16 litre NaI detector and two types of Ge detectors. Known nuclear data was used to identify γ-rays from 42 different radionuclides in the recorded spectra.

A computer code has been developed to simulate a briefly irradiated uranium sample source (with full retention of fission products) and the spectra produced by a sodium iodide (NaI) detector in close proximity to this source. The simulation has been compared to the experimental data set spanning the time period 3 hours to 11 months after the irradiation. The agreement is good.

The code can be used to model different detector geometries (ie: airborne measurements of deposited material) and radiation histories. The code can be readily developed to model other source terms (eg: by including neutron activation of reactor materials and the differentiation of fission products). It could be used to model the response of AGS systems to past accidents and to reference accidents for current nuclear power plants.

The NaI spectra obtained from the experimental measurements and computer simulations offer the promise that in the event of an atmospheric release and subsequent deposition from a nuclear reactor accident the relative concentrations of individual radionuclides, and radiologically important groups of nuclides, could be identified by further development of the airborne radiometric survey technique.

Using this technique measurements would be rapid and superior in coverage to land based methods (Sanderson et. al. 1995a, b). In addition to total γ-ray dose rates, volatile radionuclides (eg: noble gases), semi-volatile radionuclides (eg: iodine, tellurium and caesium) and non-volatile radionuclides (eg: niobium and lanthanum) could be measured using NaI detector systems, with appropriate spectral deconvolution methods.

The use of cryogenically cooled Germanium detectors would give higher resolution but produce greater operational difficulties in their use. Further work would be needed to answer questions relating to lower counting statistics and the manner in which such spectra might complement and enhance data collected with NaI detectors.

6. REFERENCES

Allyson J.D. (1994) 'In-situ and aerial environmental radioactivity measurements: An investigation of some factors relating to calibration by simulation and experiment.', Ph.D. Thesis, University of Glasgow.

Allyson J.D., Sanderson D.C.W (1997) 'Monte Carlo simulation of environmental airborne gamma-spectrometry.', Journal of Environmental Radioactivity, in print.

Allyson J.D. (1997) Private Communication, paper in preparation.

Bristow Q. (1978) 'The application of airborne gamma-ray spectrometry in the search for radioactive debris from the Russian satellite Cosmos 954 (Operation "Morning Light").' Geol. Surv. Can. paper **78-1B**, 151-162.

Cresswell A.J. (1997) 'GRAFIC - Gamma Ray And Fission Inventory Code.', SURRC internal report.

Grasty R.L. (1980) 'The search for Cosmos-954.', Search Theory and Applications, Plenum Press, New York, 211-220.

Grasty R.L., Hovgaard J., Multala J. (1997) 'Airborne gamma-ray measurements in the Chernobyl plume.', Decision Making Support for Off-sit Emergency Management, Proceedings of the Fourth International Workshop on Real Time Computing of the Environmental Consequences of an Accidental Release from a Nuclear Installation, 225-230.

Mellander H. (1989) 'Airbourne gamma spectrometric measurements of the fall-out over Sweden after the nuclear reactor accident at Chernobyl, USSR.', IAEA/NENF/NM-89-1.

OECD (1994) 'JEF-PC A Personal Computer Program for Displaying Nuclear Data from the Joint Evaluated File Library', OECD Nuclear Energy Agency.

Paatero P. (1964) 'DRIFT - A drift-correcting computer subroutine for nuclear spectroscopy.', Nuclear Instruments and Methods **31**, 360.

Sanderson D.C.W., Allyson J.D., Tyler A.N., Scott E.M. (1995a) 'Environmental applications of airborne gamma spectrometry.' Application of Uranium Exploration Data and Techniques in Environmental Studies. Proceedings of a Technical Committee meeting held in Vienna, 9-12 November 1993. IAEA-TECDOC-827, 71-91.

Sanderson D.C.W., Allyson J.D., Tyler A.N. (1995b) 'Rapid quantification and mapping of radiometric data for anthropogenic and technologically enhanced natural nuclides.' Application of Uranium Exploration Data and Techniques in Environmental Studies. Proceedings of a Technical Committee meeting held in Vienna, 9-12 November 1993. IAEA-TECDOC-827, 197-216.

Sanderson D.C.W., Cresswell A.J., Allyson J.D., McConville P. (1997) ‘Review of past nuclear accidents: source terms and recorded gamma-ray spectra.’, DOE/RAS/97.001

Williams D., Cambray R.S., Maskell S.C. (1958, declassified 1984) ‘An airborne radiometric survey of the Windscale area, October 19-22 1957.’, EL/R2438 UKAEA.

APPENDIX A: Details of Measurements Taken.

Date	Start time	Source	Source-NaI Distance (cm)	AGS rack			Ortec 919 buffer		
				Number of readings	Livetime (s)		Number of readings	Livetimes (s)	
					NaI	GMX		GMX	LoAx
11/9/95	1420	B/grd	164	4	30	100			
	1425	A		48					
12/9/95	0915	Blank		9					
	1025	A		4					
	1040	B		4					
	1055	Blank		4					
	1110	Calib.		4					
12/9/95	1420	Calib	68	1	300	600	1	300	300
	1435	B/grd		2			1		
	1500	B		91			3		
13/9/95	1015	Blank		3			1		
	1040	A		3			1		
	1120	B/grd		3					
13/9/95	1220	E	164	12	300	1000	1	300	1000
	1530	B/grd		5			1		
	1655	E		60			2		
14/9/95	1105	Blank		4			1		
	1230	Calib.		1			1		
14/9/95	1620	Calib.	164	4	300	1000	1	1000	1000
	1715	B/grd		2					
	1735	E		160			3		
16/9/95	1605	B/grd		2					
16/9/95	1640	E	164	314	300	1000	20	10000	10000
21/9/95	2010	E	60	34	600	2000	28	10000	10000
25/9/95	1040	Blank	60	6	600	2000	1	10000	10000
	1340	E		406			79		
6/10/95	1720	E	60	116	600	2000	23	10000	10000
10/10/95	1110	Blank		177			1		
13/10/95	2245	E	60	715	300	1000	80	10000	10000
23/10/95	1310	Blank		284					
31/10/95	1115	E	60	52	600	2000	9	10000	10000
1/11/95	1620	E+C		76			71		
13/1195	1040	B/grd	60	89	600	2000	17	10000	10000
15/11/95	1335	C+E		380			63		
24/11/95	1345	B/grd	60	177	600	2000	55	10000	10000
1/12/95	0930	C+D+E	60	422	600	2000	80	10000	10000
11/12/95	0900	B/grd	60	127	600	2000	20	10000	10000
14/12/95	0900	C+D+E	60	522	600	2000	67	10000	10000
13/2/96	1600	Calib.	60	10	300	600	10	600	600
14/2/96	1805	C+D+E	60	383	600	2000			
21/3/96	1630	Calib.	60	10	300	600	10	10000	10000
25/3/96	0910	C+D+E	60	46	600	2000	2	10000	10000
29/3/96	1500	C+D+E	60	118	600	2000	10	10000	10000

1/4/96	0900	C+D+E	60	41	600	2000	5	10000	10000
2/4/96 3/4/96 4/4/96 16/4/96 17/4/96	0825 0710 1435 0815 1040	C+D+E B/grd C+D+E B/grd C+D+E	60	42 56 500 47 307	600	2000	2	10000	10000
29/4/96	1030 1510	B/grd C+D+E	60	8 76	600	2000	1 9	10000	10000
1/8/96 2/8/96	1650 0910 1425 1450	C+D+E B/grd Calib. C+D+E	60	29 9 1 165	600	2000	 1 1 10	10000	1800
26/8/96	1525	Calib.	60	4	300	1000	3	1000	1000
26/8/96	1655	B/grd	60	27	600	2000	4	10000	10000
27/8/96	0900	C+D+E	60	45	600	2000	4	10000	10000

APPENDIX B: Detector Gain Drift Measurements and Correction Technique.

During the analysis of the NaI spectra recorded during the experiment it was noted that the detector gain drifted considerably. A computer program, in C++, has been developed to monitor and correct the gain drift in spectra written in the format used by existing AGS programs. The gain drift, the method used to monitor and correct for it, and the code are described.

B.1 Measurement of Gain Drift.

The gain drift was monitored by measuring the channel of the peak maximum for the 1461keV gamma-ray from ^{40}K and the 2614keV γ-ray from ^{208}Tl. These were determined by finding the maximum channel within the K and Tl windows (channels 220-270 and 390-480 respectively) and then fitting a straight line to the differential of the spectrum around this point, using 7 points for the K peak and 11 for the Tl. This is illustrated in figure B.1, and is achieved in the code by the function `get_chn'.

This routine takes four input variables; the low and high limits of the peak window (roi_low and roi_high), the spectrum number (either 1 or 2, the AGS system records two spectra in each file) and the number of channels either side of the peak maximum to use for the linear regression (num_chn). It smooths the spectrum within the peak window (either spec1[] or spec2[] depending on spc_num) over three channels into spec[], and then differentiates it into spec_d[]. The channel

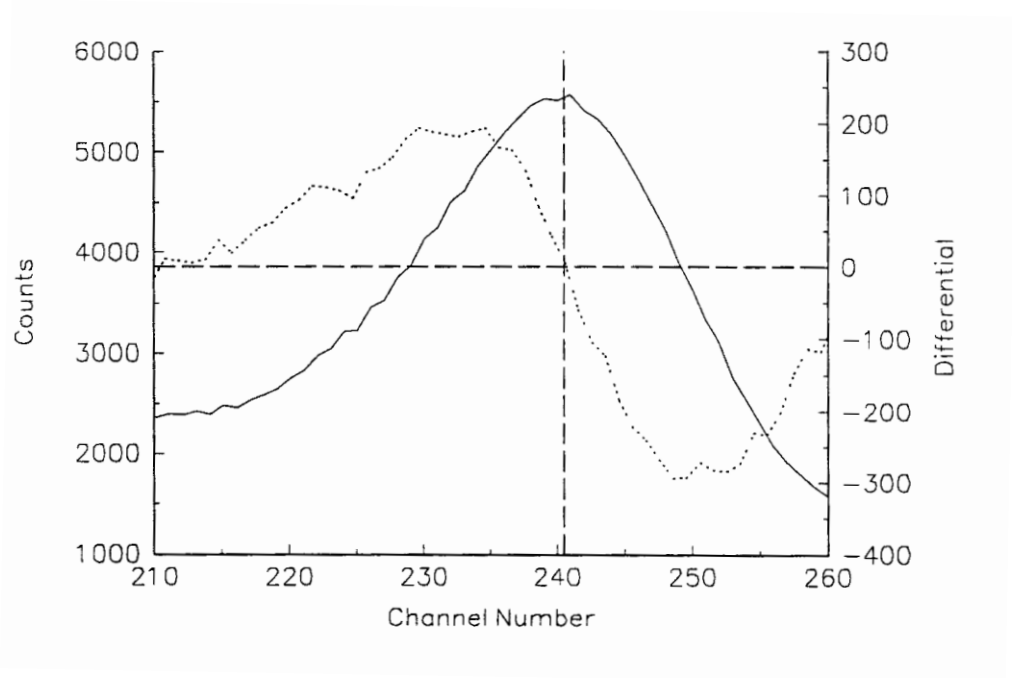

Figure B.1: Illustration of the peak maximum determination method. The maximum of the spectral peak (solid curve) is determined from the interception of the differential (dashed curve) with the zero axis, using a linear regression.

corresponding to the peak maximum is then found. A linear regression of the differential around this channel using (num_chn*2)+1 points is then carried out to determine the intercept (xm-a*ym) which is returned as the peak channel.

```
float get_chn(int roi_low, int roi_high, int spc_num, int num_chn)
{

  int x, j, pk_chn, m;
  long xx;
  float y, yy, xy, xm, ym, a, pk_counts=0;

  for(j=roi_low; j<(roi_high+1); j++)
    {
      if(spc_num==1) spec[j]=(spec1[j-1]+spec1[j]+spec1[j+1])/3;
      else spec[j]=(spec2[j-1]+spec2[j]+spec2[j+1])/3;    //smooth
      spec_d[j]=spec[j]-spec[j-1];    //differential
      if(spec[j]>pk_counts)
       {
         pk_counts=spec[j];
         pk_chn=j;    //channel of peak max.
       }
    }
  x=xx=y=yy=xy=m=0;
  for(j=(pk_chn-num_chn); j<(pk_chn+num_chn+1); j++)  //linear reg.
    {
      x+=j;
      xx+=pow(j,2);
      y+=spec_d[j];
      yy+=pow(spec_d[j],2);
      xy+=(spec_d[j]*j);
      m++;

     }
   xm=x/m;
   ym=y/m;
   if((xy-x*y/m)==0) return pk_chn;  //trap divide by zero
   a=(xx-(pow(x,2)/m))/(xy-x*y/m);
   return(xm-a*ym);  //return intercept
}
```

B.2 Variation of Gain.

The peak channels for the ^{40}K and ^{208}Tl γ-rays were measured for the spectra recorded using the aerial survey NaI detector in the laboratory. These channels were then plotted against time, and the variation noted. Figure B.2 shows this variation over a single set of measurements. It is evident from these plots that the gain followed a diurnal cycle, increasing during the night and decreasing during the day. There was also a weekly cycle with the gain increasing at weekends. The peak maximum varies by up to 10 channels for the ^{40}K peak and 20 channels for the ^{208}Tl peak, approximately 5%.

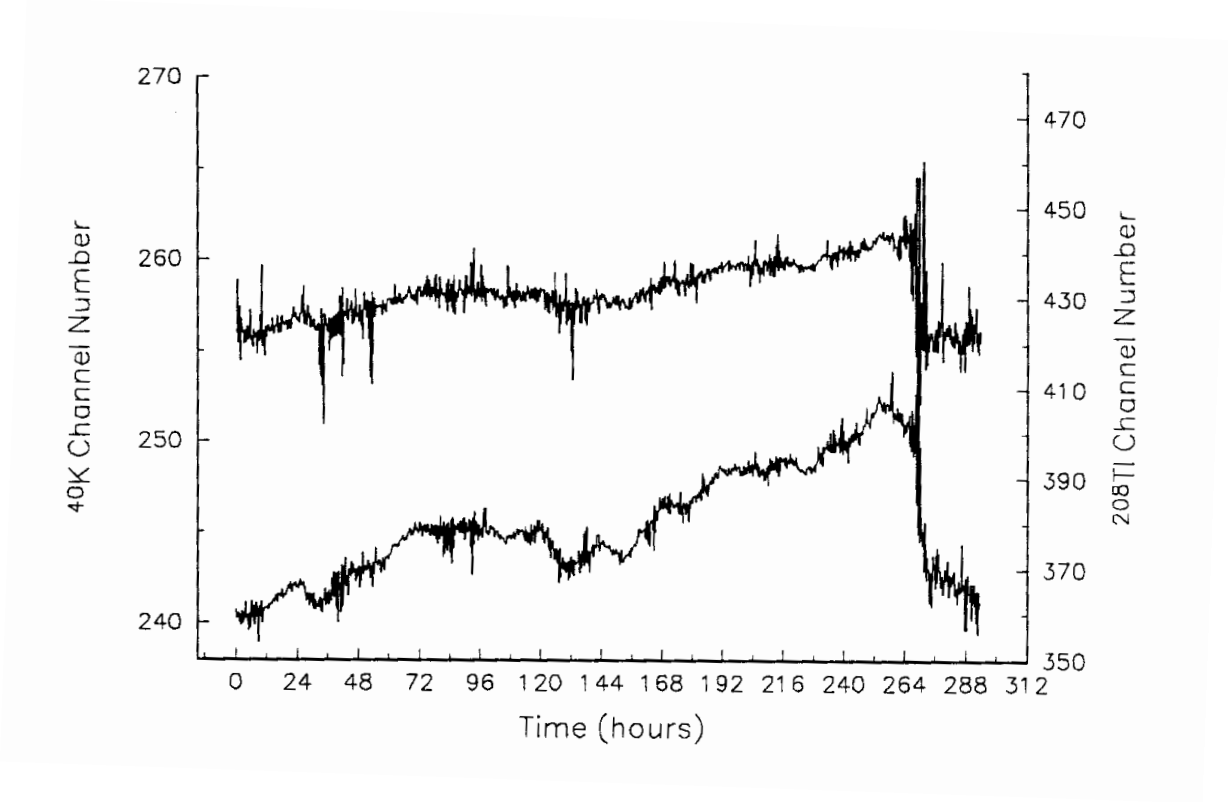

Figure B.2: Variation of gain for the ^{40}K (bottom curve) and ^{208}Tl (top curve) over a 12 day interval commencing 0920 on Thursday 14th December 1995.

B.3 Correction of Gain Drift.

The gain drift was corrected using a routine based on the DRIFT subroutine of Paatero 1964. This calculates a stretch and shift to fit two peaks to desired positions, here Tl_tar=435.8 and K_tar=242.5 are the desired channels for the Tl and K peaks to fit the spectrum to exactly 6 keV per channel. The stretch factor is the difference between the desired positions of these two peaks divided by the actual difference. The shift factor is then calculated for one of the peaks, being the difference between the desired channel and the actual channel times the stretch factor.

When correcting the spectrum a new channel number is produced by multiplying the old channel number by the stretch factor and adding the shift factor. This new channel number is unlikely to be an integer, and so the contents of the old channel are divided between two new channels depending on the difference between the new channel number and its modulus.

The routine uses the mean values for the Tl and K peaks for the current and previous 5 readings, K->get_mean() and Tl->get_mean(), using a stack class (a class is a C++ programmer defined data structure). The section of code given below gain corrects spec2[] writing the corrected spectrum to new_spec2[], a similar section gain corrects spec1[].

```
stretch=(Tl_tar-K_tar)/(Tl->get_mean()-K->get_mean());
shift=K_tar-(K->get_mean()*stretch);  //calc. shift&stretch
for(j=0; j<504; j++) new_spec2[j]=0;
for(j=0; j<504; j++)
  {
    a=(j*stretch)+shift;
    if((a>=0)&&(a<503))
     {
        new_spec2[a]+=((1+(int) a)-a)*spec2[j]; //write new spectrum
        new_spec2[a+1]+=(a-(int) a)*spec2[j];
      }
  }
```

The complete code reads the data files, storing the header sections and writing the two NaI spectra into spec1[] and spec2[]. It then does the gain correction, and writes the gain corrected spectra to file in the format used by the AGS software (using the original header sections). It also allows for the subtraction of a background, the writing of a file giving the un-corrected peak positions and the summation of several spectra.